

Turbulent molecular clouds

Patrick Hennebelle · Edith Falgarone

Received: September 15, 2012 / Accepted : October 10, 2012

Abstract Stars form within molecular clouds but our understanding of this fundamental process remains hampered by the complexity of the physics that drives their evolution. We review our observational and theoretical knowledge of molecular clouds trying to confront the two approaches wherever possible. After a broad presentation of the cold interstellar medium and molecular clouds, we emphasize the dynamical processes with special focus to turbulence and its impact on cloud evolution. We then review our knowledge of the velocity, density and magnetic fields. We end by openings towards new chemistry models and the links between molecular cloud structure and star-formation rates.

Keywords Instabilities · Interstellar medium: kinematics and dynamics – structure – clouds · Star: formation

1 Introduction: bridging theory and observations

In the Galaxy and all spiral galaxies, molecular clouds are the sites of star-formation. The roots of star-formation are therefore to be sought in the physics of these clouds. We review our current understanding of the physics of molecular clouds both from a theoretical and observational point of view, trying to systematically confront the two approaches. Such a confrontation turns out to be more difficult a task than anticipated because on the observational and theoretical sides, the concept of molecular clouds relies on different foundations: in the former, molecular clouds are by definition structures detected in molecular line emission, mostly that of CO because H₂ is not easily accessible to observations; in the latter,

Patrick Hennebelle
Laboratoire AIM, Paris-Saclay, CEA/IRFU/SAP - CNRS - Université Paris Diderot, 91191,
Gif-sur-Yvette Cedex, France
E-mail: patrick.hennebelle@cea.fr

Edith Falgarone
LERMA, CNRS, Ecole Normale Supérieure & Observatoire de Paris, 24 rue Lhomond, 75231
Paris Cedex, France
E-mail: edith.falgarone@ens.fr

molecular clouds are structures denser and more shielded from the UV field than atomic and diffuse gas. In this review, we will see that molecular gas is not necessarily dense and shielded from UV photons, that gas with only traces of H_2 can harbor large amounts of molecules other than H_2 , and that CO, the traditional and powerful tracer of molecular gas in the universe, is indeed a complex tracer. Another difficulty on bridging observations and theory stems from the projections of the observations (line-of-sight velocities, densities providing only column densities), not to mention those involved in the observations of magnetic fields. These projections make local quantities hard to derive, the inversion of the observables relying on assumptions (homogeneity, geometry) and theoretical knowledge (collisional excitation cross-sections of molecules, interstellar chemistry, line radiative transfer, ...).

Observations of molecular clouds in the Galaxy now cover an impressive range of size scales, from a few 100 pc to the milli-pc scale. The less controversial facts are: (i) scaling laws are found to relate the masses, sizes and internal velocity dispersions of clouds across this range of scales, hence the physics of molecular clouds involves all of them; (ii) molecular clouds, as traced by CO, include self-gravitating and non self-gravitating structures; (iii) to be understood, the interplay of gravity and turbulence has to be put on even larger size scales (galactic dynamics, galaxy interactions, ...) as shown by new observational capabilities (Swinbank et al. 2010, Herrera et al. 2012).

Significant theoretical progress has been accomplished during the last decades. This has been largely, though not exclusively, permitted by the development of numerical simulations which, thanks to the increase of computing power but also to the use of new numerical schemes (such as adaptive mesh refinement) can now cover a broad range of scales. In parallel, much effort has been made to treat the important physical processes involving magnetic fields, radiative transfer and chemistry, which are now commonly incorporated into numerical simulations.

In spite of these achievements, we are still far from a proper modeling of the molecular clouds. This is because the dynamics of scale than can be tackled in the simulations remains far too restricted. As an example, while the effective Reynolds number (see definition in Section 3.1) of the numerical simulations is certainly not larger than $\simeq 10^4$, its value within molecular clouds is larger than $10^6 - 10^7$. Moreover, molecular clouds, as we will argue later on, are not isolated entities, but are dynamically linked to their environment. This makes the limitation of the range of scales treated in simulations even more severe, since ideally one should treat not only the molecular clouds but also the diffuse interstellar medium in which they form and are embedded.

While the broad range of scales is certainly a severe issue, the complexity of the physical processes is the other outstanding difficulty that interstellar medium (ISM) studies are facing. It is well known, for instance, that in the ISM, thermal, kinetic, magnetic, radiative and cosmic ray energies are all on the order of $\simeq 1 \text{ eV cm}^{-3}$ (within one order of magnitude). This energy equipartition suggests that these processes are coupled to each other. Adding self-gravity for the densest parts of the interstellar gas, this makes six *fields of knowledge*, which are interacting in the cloud evolution and the star-formation process.

Given this complexity, it is not a surprise that outstanding resilient questions remain, among which:

- Are molecular clouds well described by turbulent density fluctuations (*e.g.* Ballesteros-

Paredes et al. 1999)?

- Is the observed hierarchy the outcome of gravitational fragmentation or of large scale dynamics imposed by the galactic environment (*e.g.* Chièze 1987, Koyama & Ostriker 2009)?
- Is gravity feeding turbulence throughout the hierarchy (*e.g.* Field et al. 2008)?
- What is the nature of the non-thermal pressure? How does it act (*e.g.* Bonazzola et al. 1987)?
- What is the evolutionary path between atomic gas and giant molecular clouds (*e.g.* Koda et al. 2009)?
- Are molecules a prerequisite to star formation (*e.g.* Glover & Clark 2012)?
- What is the role played by stellar feedback in the evolution of molecular clouds (*e.g.* Blitz & Shu 1980)?

A complete and detailed overview of the subject is beyond the scope of these pages and we had to make choices. We put special emphasis on the dynamic processes and present the different theories directly used to interpret relevant observations. When possible, we try to give some hints of how the theoretical relations are inferred and their physical significance. Numerical simulations are discussed, particularly when their results can be confronted to theory. However, given the large number of relevant works in this area, our review is by no means exhaustive. The same applies to the observations, more attention have been given to observations from which statistics are inferred and then confronted to theories. We also stress that, while the primary focus of the present review is not star-formation, we will address closely related topics, such as the origin of the core mass function and the derivation of the star-formation rate, because they are integral parts of molecular cloud physics. Other comprehensive references on closely related topics can be found in Mac Low & Klessen (2004), Elmegreen & Scalo (2004), Scalo & Elmegreen (2004), McKee & Ostriker (2007) and Kennicutt & Evans (2012).

The review is divided in seven sections. Section 2 provides a broad overview of our observational knowledge of molecular clouds in the Galaxy and presents a plausible formation scenario. Section 3 is dedicated to the turbulent velocity field and its impact on the cloud physics. The density structure and mass distribution are discussed in Section 4 with subsections devoted to filaments and dense cores. Section 5 focuses on magnetic fields. Section 6 presents openings and stress the key role played by turbulence. In the last section (section 7) conjectures and questions left open are discussed.

2 Overview: the broad concept of molecular clouds

2.1 Traditional tracers of molecular clouds

Molecular clouds have been discovered in the 1970s via their emission in the J=1–0 transition of CO at $\nu = 115\text{GHz}$ (Wilson et al. 1970, Penzias et al. 1972). The beauty of this discovery lies in the fact that two lines (those of the two main isotopologues ^{12}CO and ^{13}CO) and the knowledge of the CO spectroscopy were sufficient to infer that the line emitting gas in dark clouds (*i.e.* those seen as dark islands on visible maps of the sky) was cold ($T_K < 10\text{K}$) and dense ($n > 10^3\text{cm}^{-3}$) and that the CO abundance relative to H_2 was low, $[\text{CO}]/[\text{H}_2] < 10^{-4}$. This was a

powerful discovery: a trace molecule was found to be a strong line emitter, opening the possibility of surveys. The first CO surveys of the Galactic plane (Solomon et al. 1987, Dame et al. 1987) brought to light the existence of CO-bright and massive entities, called the giant molecular clouds (GMC), most of them harboring star forming regions.

More sensitive and fully sampled surveys (Dame et al. 2001) revealed a weaker, so called “cold” CO emission bridging the CO-bright islands of the GMCs in space and velocity, covering the inter-arm regions and extending beyond the galactic plane. A faint thick molecular disk was discovered, with a scale height (~ 250 pc) comparable to that of the HI layer in the inner Galaxy (Dame & Thaddeus 1994). Moreover, the mass comprised in the “cold” CO component was estimated to be larger than that comprised in all the GMCs, a result that in the 1980s raised a long and vivid controversy. At the same epoch, HI superclouds were found as very large scale structures in the Galaxy (several 100 pc), each comprising several GMCs (Elmegreen & Elmegreen 1987) setting the large scale environment of what was then understood as molecular clouds. Since then, several $^{12}\text{CO}(1-0)$ (May et al. 1988, 1993, Sanders et al. 1986, Clemens et al. 1986) and $^{13}\text{CO}(1-0)$ (Jackson et al. 2006) surveys have further broadened the view of molecular gas and clouds throughout the Galaxy, beyond the neighborhood of star-forming regions.

Individual GMCs (size ~ 50 pc) are now resolved in nearby external galaxies (*e.g.* Gratier et al. 2010, Egusa et al. 2011, Koda et al. 2009). Recent results obtained in $^{12}\text{CO}(1-0)$ in the grand-design spiral galaxy M51 are shown in Fig. 1. At low resolution ($4''$ or ~ 200 pc), GMC associations follow the spiral arms and at higher resolution ($0.7''$ or 30 pc) GMCs are resolved structures: some are also found between the arms (Egusa et al. 2011). Interestingly, the most massive GMCs are located downstream of the spiral arms, in close association with star forming regions, suggesting a time evolution towards star-formation across the arms. Koda et al. (2009) find that GMCs and their H_2 molecules are not dissociated upon leaving the spiral arms, which supports a long lifetime for molecular clouds and molecular gas in spiral galaxies. For comparison, the $^{12}\text{CO}(1-0)$ column density map (resolution 0.03 pc) of the nearby Taurus-Auriga complex, over the same scale of 30 pc, is shown in Fig. 1 (Goldsmith et al. 2008): it reveals the complex structure of the gas seen in $^{12}\text{CO}(1-0)$, at all scales. Unexpectedly, this complexity extends down to milliparsec scales (Falgarone et al. 1991, 2009).

Another observational technique has proven very powerful at revealing massive clouds in the central regions of the Galaxy: shadows on the bright mid-IR and near-IR stellar (and small particle emission) backgrounds of the inner Galaxy. The infrared dark clouds (IRDCs) (P erault et al. 1996, Egan et al. 1998, Hennebelle et al. 2001) appear as massive entities of large column density (N_{H} up to 10^{23} cm^{-2}) immersed in large clouds of lower extinction containing 10 times more mass (Kanulainen et al. 2011). They harbor small but massive cores (Rathborne et al. 2010, Peretto & Fuller 2010) that are occasionally associated with massive young stellar objects (YSOs). In spite of their large mass fractions at high column density, IRDCs, on average, have a low star-forming activity.

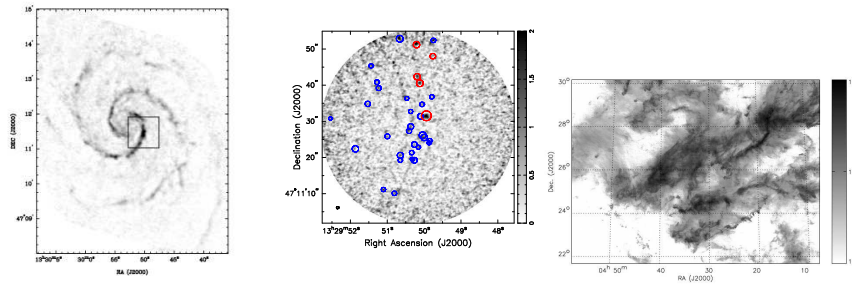


Fig. 1 $^{12}\text{CO}(1-0)$ integrated intensity maps of M51 at a resolution of ~ 200 pc (*left*) and 30 pc (*center*) within the square field shown in left panel (from Egusa et al. 2011). $^{12}\text{CO}(1-0)$ column density map of the Taurus-Auriga complex over the same size ~ 30 pc, at a resolution of ~ 0.03 pc (Goldsmith et al. 2008) (*right*). The intensity scale is logarithmic and shown in the wedge. In the white regions, $N(\text{CO}) = 7.5 \times 10^{15} \text{ cm}^{-2}$, a factor ~ 100 smaller than the maxima.

2.2 Diffuse molecular gas as a part of molecular clouds

Beyond the above surveys of molecular clouds, the high sensitivity and broad dynamic coverage of most recent observations of CO line emission (including those of the all-sky *Planck* survey) and absorption with the *Hubble Space Telescope* reveal the existence of CO molecules in environments weakly shielded from the ambient UV-field. This raises the issue of the CO molecules survival in these environments, and of the nature of the gas component that CO emission is actually tracing there. Because it is a CO-emitter and may be considered as the birth-site of dense molecular clouds, this gas component called “diffuse molecular gas” deserves attention. The following sections are dedicated to it.

On observational grounds, the definition of the diffuse neutral ISM has evolved continuously since its fortuitous discovery by Hartmann in 1904. It is now generally agreed that it is a low density medium ($n_{\text{H}} < \text{a few } 10^3 \text{ cm}^{-3}$), weakly shielded from the interstellar radiation field (ISRF) ($A_{\text{V}} < \text{a few mag}$), therefore comprising the diffuse atomic ($n_{\text{H}} \sim 50 \text{ cm}^{-3}$), diffuse molecular and translucent media, following the terminology of Snow & McCall (2006). An even broader definition includes the above plus the edges of molecular clouds as traced by their $^{12}\text{CO}(J=1-0)$ emission, *i.e.* all the gas that is not in dense cores and/or star forming regions. Equivalently, the diffuse ISM can be considered to be all material with total hydrogen column density less than a few $\sim 10^{21} \text{ cm}^{-2}$ at the parsec scale. This unified definition is motivated by the shapes of the probability distribution functions (PDF) of the column density (inferred from dust extinction) of nearby molecular clouds: they have a log-normal part from $A_{\text{V}} \sim 0.5 \text{ mag}$ up to $A_{\text{V}} \sim \text{a few magnitudes}$, and a power-law tail at higher column densities, characteristic of dense cores and filaments present only in clouds actively forming stars (Kainulainen et al. 2009). The log-normal contribution that spans two orders of magnitude in N_{H} corresponds to the diffuse ISM of the molecular clouds. The diffuse ISM, at large, may therefore be seen as all the gas that does not belong to small-scale, self-gravitating structures such as dense cores, dense filaments and star-forming regions. Note that the diffuse medium, as defined above, comprises a significant mass fraction of molecular clouds. In the Taurus complex, at the 30 pc

scale, Goldsmith et al. (2008) find that half the mass of the complex is in regions having column densities less than $2 \times 10^{21} \text{ cm}^{-2}$.

2.2.1 The diffuse ISM: A two-phase medium

The shape of the cooling function, dominated by [C II] line emission, makes the diffuse ISM thermally bistable at the pressure and metallicity conditions prevailing in the Solar Neighborhood (Field et al. 1969, Wolfire et al. 1995, 2003), *i.e.* at a distance of less than $\simeq 1 \text{ kpc}$ from the Sun. The balance between heating and radiative cooling processes generates two stable phases at very different temperatures and densities, $T \sim 100 \text{ K}$ and $n_{\text{H}} \sim 30 \text{ cm}^{-3}$ for the cold neutral medium (CNM), $T \sim 8000 \text{ K}$ and $n_{\text{H}} \sim 0.3 \text{ cm}^{-3}$ for the warm neutral medium (WNM). However, a broad range of kinetic temperatures, pervading the thermally unstable range, is usually inferred from UV absorption lines sampling the diffuse ISM (e.g. Fitzpatrick & Spitzer 1997), and recent sensitive HI observations also probe temperatures in this range (Heiles & Troland 2003, Begum *et al.* 2010). The latter infer that about half the WNM is at temperatures in the range $500 - 5000 \text{ K}$, thus evolving between the two stable phases.

2.2.2 Pressure of the diffuse ISM

Because it sits in the gravitational potential of the Galaxy and extends up to $\sim 300 \text{ pc}$ above the plane, the diffuse ISM has to be supported by a pressure that is about 10 times its thermal pressure, $P_{\text{tot}} = 3 \times 10^{-12} \text{ dynes cm}^{-2}$, or $P_{\text{tot}}/k \sim 2 \times 10^4 \text{ cm}^{-3} \text{ K}$ (Cox 2005). The non-thermal contributions to the total pressure are due to supersonic turbulence and magnetic fields, in rough equipartition, as shown by measurements of magnetic field intensity (Crutcher et al. 2010, see Section 5) and HI linewidths (Haud & Kalberla 2007). The distribution of thermal pressures in the Solar Neighborhood, inferred from [C I] fine-structure absorption lines towards nearby stars (Jenkins & Tripp 2011) peaks at about $P_{\text{th}}/k \sim 3 \times 10^3 \text{ cm}^{-3} \text{ K}$, with large fluctuations, up to several $10^4 \text{ cm}^{-3} \text{ K}$, possibly due to expanding supernova remnants. It is noteworthy that the total non-thermal pressure in the Galactic plane is of the same order as the largest values of the thermal pressure observed. This equality suggests that the non-thermal energy eventually and occasionally dissipates into thermal energy.

2.2.3 An unexpected molecular richness

These large fluctuations of thermal pressure are a sign of a complex dynamic evolution that may provide the missing important clues to understand the origin of the remarkable molecular richness found in this hostile medium, weakly shielded from UV photons (e.g. Liszt & Lucas 1998). In the case of CO, *(i)* column densities as low as a few 10^{12} cm^{-2} , smaller than that required for CO self-shielding ($N(\text{CO}) \sim 10^{14} \text{ cm}^{-2}$, van Dishoeck & Black 1988, Lee et al. 1996) have been observed in absorption in unshielded environments where $N(\text{H}_2) < 3 \times 10^{19} \text{ cm}^{-2}$ (Sonnentrucker et al. 2007); *(ii)* large fluctuations of the CO emission of diffuse gas at small scale have been found that cannot be ascribed to shielding fluctuations; *(iii)* both CO-dark and CO-overluminous diffuse molecular gas exist with respect to the standard CO-to- H_2 conversion factor (Liszt et al. 2010, Liszt & Pety 2012).

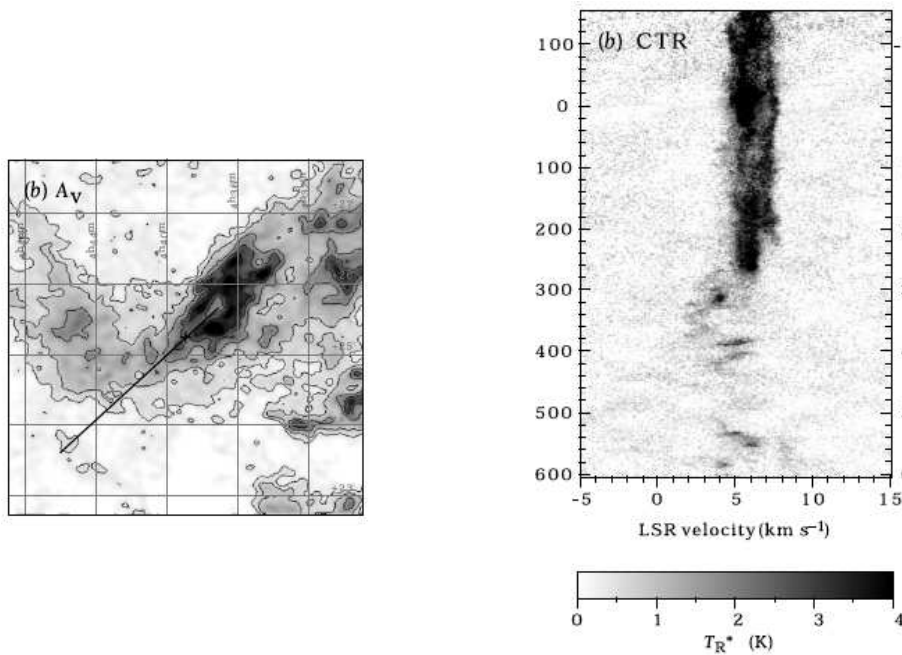


Fig. 2 Illustration of the variability of the $^{12}\text{CO}(J=1-0)$ emission along a cut across one edge of the Taurus molecular complex. (Left) the extinction map showing the position of the cut. (Right) the position-velocity diagram of the cut showing the sharp transition between translucent gas of high velocity dispersion with tiny spots of detected CO emission and the opaque part, with a much narrower velocity dispersion (from Sakamoto & Sunada 2003).

The sharp variability on arcminute scales of the CO emission of diffuse gas is primarily due to CO chemistry, a point that cannot be understood in the framework of UV-driven chemistry: small-scale gas kinematics seems to be involved. An illustration of that is shown in Fig. 2 from Sakamoto & Sunada (2003). The tiny spots of CO emission in the unshielded part of the cut across the edge of a molecular cloud are associated with large velocity variations. The authors suggest that these CO-rich structures may form through thermal instability in shocked atomic gas (Koyama & Inutsuka 2000, 2002) or Kelvin-Helmholtz (KH) instability (Sakamoto 2002) although they favor thermal instability, given the long timescale for the growth of the KH instability. Barriault et al. (2010) investigate the transition between atomic and molecular gas in high-latitude clouds. They find that there is no systematic coincidence between IR-excess (*i.e.* FIR emission in excess to that predicted from HI column density) and CO emission and that CO appears where two HI velocity components merge or where a large velocity-shear is present in the HI map. These results strengthen the possibility of a new CO formation route linked to the dynamics of the HI gas (see Section 6.1.2).

Recently, the molecular richness of the diffuse medium has been further illustrated by absorption spectroscopy in the submillimeter domain against the dust emission of bright star-forming regions in the Galaxy. Small hydrides, the building blocks of IS chemistry, have been detected with unexpected large abundances. Several species provide unique clues to our understanding of the physics of the dif-

fuse ISM: the large excess of OH^+ over H_2O^+ implies that these ions are formed in mostly atomic gas (Gerin et al. 2010, Neufeld et al. 2010a); the ubiquitous HF is a powerful tracer of H_2 in diffuse gas because of the highly exothermic reaction of fluorine with H_2 (Neufeld et al. 2010b, Sonnentrucker et al. 2010); the large abundances of CH^+ and SH^+ both with highly endoenergetic formation routes reveal the existence of local reservoirs of energy, exceeding by far that provided by UV-photons (Falgarone et al. 2010a,b, Godard et al. 2012). Last, the molecular fraction of the diffuse medium $f_{\text{H}_2} = N(\text{H}_2)/(N(\text{H}) + 2N(\text{H}_2))$ where these hydrides are observed is found to fluctuate by large factors (Godard et al. 2012), from less than 0.1 to almost unity, further blurring the distinction between atomic and molecular clouds.

In summary, CO is not exclusively a tracer of dense gas and its formation rate may be enhanced by the gas dynamics. Moreover, molecular gas exists without associated CO emission. This may bring partial answers to the persistent questions raised on the CO-to- H_2 ratio.

2.3 The CO-to- H_2 ratio

The first major achievement of CO observers has been the determination of the well known CO-to- H_2 conversion factor, $X_{\text{CO}} = N(\text{H}_2)/W(\text{CO})$ that provides the only way to measure the amount of molecular hydrogen (which cannot be observed directly in cold environments, see Section 6.1.1) from the integrated ^{12}CO line emission, $W(\text{CO})$. Estimates of total gas masses (atomic and molecular) were then made possible, an essential step forward to unravel the physics of molecular clouds. The standard value $X_{\text{CO}} = 2 \times 10^{20} \text{ cm}^{-2}/(\text{K km s}^{-1})$ was calibrated on X-ray and near-IR extinctions towards the central regions of the Galaxy, therefore kpc-long sight lines encompassing GMCs, dark and diffuse clouds. The X_{CO} factor was inferred by subtracting the contribution of the atomic gas to the total extinctions.

Two recent space experiments *Fermi/LAT* in the γ -ray domain (Abdo et al. 2010, Ackermann et al. 2011) and *Planck* in the submillimeter domain (Planck collaboration et al. 2011) independently confirm what was already found by the first γ -ray space mission, *COS B* (Lebrun et al. 1983): there are significant amounts of molecular gas in the Galaxy that are not traced by ^{12}CO and would be atomic gas rich in H_2 without detectable CO emission (e.g. Grenier et al. 2005). This CO-quiet H_2 gas lies at the periphery of known bright molecular complexes, a fact consistent with model predictions (Wolfire et al. 2010). In the case of *Fermi/LAT*, excesses of γ -ray emission are observed in these regions that cannot be ascribed to higher densities of cosmic rays because these are accurately measured. In the case of *Planck*, the dust optical depth excess above that expected from known HI and CO emission occurs in regions where $8 \times 10^{20} \text{ cm}^{-2} < N_{\text{H}} < 5 \times 10^{21} \text{ cm}^{-2}$, typical of the diffuse molecular gas. The mass of CO-quiet gas in the Solar Neighborhood is estimated to be about 30% of its atomic gas and 100% of the CO-bright gas.

Both groups, however, discuss the large uncertainties due to underestimates of the HI optical depth in molecular clouds, *i.e.* overestimation of the spin temperature. Indeed, atomic hydrogen at very low temperatures is found in molecular clouds (Li & Goldsmith 2003). If the amount of HI has been underestimated in the calibration of the X_{CO} factor in the Galaxy, H_2 would be overestimated and

X_{CO} is indeed too low. This would be the origin of the subsequent underestimate of H_2 associated to a given CO observation.

A fact that has not always been fully appreciated is that CO emission from diffuse gas leads to the same CO-to- H_2 conversion factor as in dense clouds (Liszt & Pety 2012). This can be understood in the framework of radiative transfer: the radiation efficiency of CO per molecule in low-density gas is much higher, because collisional de-excitation is weak and each collisional excitation is followed by a radiative de-excitation.

In the following sections, we will see that molecular clouds do not have the same characteristics whether they are traced by $^{12}\text{CO}(1-0)$ emission, $^{13}\text{CO}(1-0)$ emission (almost 100 times less optically thick) or by emission of high dipole moment species (such as CS, CN...) that are specific high density tracers ($n_{\text{H}} > 10^5 \text{ cm}^{-3}$). The diffuse component discussed above enters the concept of molecular clouds because it is locally CO-rich, contributes to the ^{12}CO emission of molecular clouds at a significant level, and because it comprises a large fraction of their mass. Finally, it is a highly dynamic component that plays a key role, as will be seen, in the formation of dense molecular clouds.

2.4 Link between molecular clouds and their large scale environment

The connection between molecular clouds and their surrounding ISM in galaxies is an important issue because molecular clouds (*i*) presumably form out of their diffuse environment; and (*ii*) evolve by interacting with it.

2.4.1 The HI halos and the molecular cloud phases

Many, if not all, molecular clouds are embedded into massive halos detected in the HI 21 cm line, therefore containing a significant fraction of atomic hydrogen (Hasegawa et al. 1983, Wannier et al. 1983, Elmegreen & Elmegreen 1987). Early on, the mass within these HI halos has early been estimated to be comparable to (or even greater than) the mass within the molecular clouds themselves. While Hasegawa et al. (1983) proposed that the HI halo constitutes the accretion reservoir of the molecular clouds, Wannier et al. (1983) argue that the atomic hydrogen around molecular clouds is warmer than in the rest of the Galaxy and proposed that it is photo-dissociated H_2 induced by the star formation within the molecular clouds.

These observations remain difficult to perform in the Galaxy because of the confusion along the line of sight, HI being ubiquitous. However, the velocity field allowed Elmegreen & Elmegreen (1987) to identify about 30 massive HI superclouds in the first quadrant of the Galaxy, each surrounding groups of known GMCs detected in CO. These HI superclouds are found to be distributed along spiral arms with separations ($\sim 1.5 \text{ kpc}$) much larger than their size ($\sim 200 \text{ pc}$). Their mass ranges between 10^6 and $4 \times 10^7 M_{\odot}$, the mean number density is $\sim 10 \text{ cm}^{-3}$ and they are self-gravitating. Substantial effort has been made to conduct similar observations in external galaxies.

The Large Magellanic Cloud (LMC), has the advantage of being not too distant and seen nearly face on, therefore limiting the issue of the confusion. Wong

et al. (2009) studied in detail the correlation between the CO and the HI distribution. In particular, they stress that while the CO peaks are always associated to a peak in HI, there are many HI peaks in which CO is not detected. The reason is not well understood yet: it may simply be a time-scale issue or a consequence of different physical conditions. This tends to support the view that molecular clouds form out of the HI instead of HI being photo-dissociated H₂.

Whether the gas traced by HI is accreting onto molecular clouds is still an open issue and Kawamura et al. (2009) address this question in the LMC with the following approach. They have classified clouds into three categories: (1) clouds in which massive stars are not observed, (2) clouds with massive stars but no cluster, and (3) clouds with clusters. Kawamura et al. (2009) propose that this is an evolutionary sequence and they estimate that each phase lasts, respectively, 6, 13 and 7 Myr. A possible key point is that they observe that the mean mass of the third category is a few times larger than the mean mass of category I and II. If this evolutionary scenario is confirmed, it would imply that GMCs in the LMC are indeed accreting. Fukui et al. (2009) estimate the gas density in the HI halos to be of the order of 10 cm⁻³ with an accretion velocity less than 7 km s⁻¹, *i.e.* the rms velocity dispersion of the HI clouds. This leads them to estimate the accretion rate to be at most 0.05 M_⊙ yr⁻¹. The GMCs within the LMC appear to be similar to those within the Galaxy (Hughes et al. 2010), therefore seemingly suggesting that the processes are reasonably similar in these two galaxies.

M33 is a low-metallicity gas-rich nearby blue spiral galaxy much further away from the Milky Way (840 kpc). It has been mapped in CO(2-1) and HI over a radius of 8.5 kpc (Gratier et al. 2010). The HI mass (1.4×10^9 M_⊙) is five times larger than that of the molecular gas inferred from CO. At the resolution of the observations ~ 100 pc, the correspondence between the CO and HI patterns is excellent. Gratier et al. (2012) have analysed the molecular clouds in M33. They also distinguish three categories of clouds similar to the classification of Kawamura et al. (2009) and reach close conclusions.

2.4.2 What is filling the volume between molecular clouds ?

Quite early on, it was recognized that the mean density of the GMC (about 10 cm⁻³ at the 100 pc scale) inferred from their CO column density and size was much lower than the gas density, of the order of 10³ cm⁻³ or more, required to excite the observed bright CO lines (Blitz & Thaddeus 1980, Pérault et al. 1985). It was then inferred that the filling factor of dense gas within GMCs is significantly below unity, raising the question on the nature of the gas filling the volume between the CO-bright structures, *i.e.* the interclump medium (ICM)¹. Indeed, the density and temperature of the ICM presumably controls the evolution time-scale of molecular clouds and contributes to the formation, confinement, and survival of the dense clumps that eventually form stars.

The recognition that dense gas in molecular clouds was filling only a small volume, prompted the emergence of GMC models in which dense fragments were virialized in the gravitational potential well of the GMC (*e.g.* Scalo & Pumphrey

¹ Here, as a tribute to the observers community, we introduce the poor and ill-defined concept of *clump*. Let us say that a clump has an average density larger (or even much larger) than that of the CNM at the ambient pressure, and, by contrast, the ICM has much lower densities.

1982). The GMC lifetime was thus considerably extended because the observed large velocity dispersion of the GMC was no longer turbulent and supersonic (with respect to the cold cloud material) and no longer expected to dissipate within one GMC turnover time, $\sim 10^7$ yr. In this picture, the fragment boundaries were sharp density fall-offs, set by the thermal instability between the CNM and WNM (Falgarone & Puget 1985) and their orbital velocities were therefore transonic with respect to the WNM: only the rare collisions among fragments were controlling the dissipative GMC evolution. Falgarone & Puget (1986) refined this concept by introducing the magnetic field lines connecting the fragments which provided a mechanism to feed the internal turbulent energy of fragments by pumping energy from their orbital motions. The dissipation time scale of turbulence within fragments was thus lengthened to that of the quasi-virialized stage of the large scale. In this scenario, the low-density medium was the WNM, at ~ 8000 K, heated mainly by ion-neutral friction caused by the field lines entrained in the fragment motions. Such a scenario provides molecular clouds with an internal structure that closely resembles that of the diffuse ISM with both cold and warm material, but with the cold phase reaching higher densities.

In an attempt to probe the nature of the ICM medium, Williams et al. (1995) studied the Rosette molecular clouds and the correlation between CO and HI emission. They found that both are clearly anti-correlated therefore showing their association. From the HI line integrated emission, they inferred an ICM density, $\sim 4 \text{ cm}^{-3}$, 100 times lower than that of the clumps, a value somewhat plagued by the unknown geometry of the medium since only the column density is measured. From the HI linewidths, they inferred an ICM velocity dispersion of $\sim 10 \text{ km s}^{-1}$, providing the ICM with a ram pressure, $\rho\sigma^2$, comparable to the internal turbulent pressure of the clumps. They proposed that the clumps be confined by the ICM ram pressure. Unfortunately, they could not place constraints on the ICM temperature and assumed it to be $\sim 20 \text{ K}$. Such a low temperature is unlikely because it would imply that the gas thermal pressure would be about 100 K cm^{-3} , roughly 30 times below the mean ISM pressure, allowing the external ISM to penetrate into the GMC. Part of the ICM is therefore likely much warmer than 20 K and/or turbulent, providing molecular clouds with a structure that resembles that of the diffuse medium. Magnetic fields are also contributing to the pressure of the ICM and an alternative possibility is that the ICM is indeed cold, diffuse and highly magnetized. In the next section, we describe how numerical simulations are presently able to tackle this huge range of densities and temperatures.

2.5 A scenario for the formation of molecular clouds

Numerical simulations are now able to capture many of the steps leading to the formation of molecular clouds out of the diffuse ISM. The first step has been the study of the non-linear development of thermal instability triggered either by a converging flow of WNM (Walder & Folini 1998, Hennebelle & Pérault 1999, 2000, Sánchez-Salcedo et al. 2002, Audit & Hennebelle 2005, 2010, Heitsch et al. 2005, 2006, Vázquez-Semadeni et al. 2006, Hennebelle & Audit 2007), or by shocks propagating in the WNM (Koyama & Inutsuka 00, 02, Inoue et al. 2009) or by turbulent driving in the Fourier space (Seifreid et al. 2011). The conclusions common to all these studies are: (i) the WNM flow quickly breaks-up into a

multi-phase medium with dense clumps (CNM) confined by the warm external medium (WNM); *(ii)* the statistics of these clumps have strong similarities with what has been inferred for the CO clumps (discussed in Sect 3.5); *(iii)* there is a significant fraction of thermally unstable gas whose existence is made possible by the turbulent fluctuations (*e.g.* Gazol et al. 2001); *(iv)* the various phases are tightly interspersed; *(v)* the cold phase is maintained supersonic (with respect to its own sound speed) and with a velocity dispersion equal to a fraction of the WNM sound speed. Simulations including the magnetic field have also been performed. Although magnetic fields definitely modify the fluid dynamics, the above conclusions remain qualitatively similar.

In the second step, gravity has been introduced therefore letting the condensations to proceed further (Vázquez-Semadeni et al. 2008, Heitsch et al. 2008, Hennebelle et al. 2008, Banerjee et al. 2009). Fig. 3 shows a snapshot (column density, density, temperature and magnetic field cut) of a colliding flow simulation (similar to what is presented in Hennebelle et al. 2008 and Klessen & Hennebelle 2010) aiming at forming a molecular cloud. The dense gas (*i.e.* the clumps) has formed out of the diffuse gas. The structure of the cloud is made of dense and cold clumps embedded in a warmer and more diffuse gas. Gravitational collapse has occurred in a few places. As visible in the snapshot, at a few locations, the temperature abruptly varies from 10^4 to 10 K. The field shown in Fig. 3 is part of a larger cloud that contains the WNM shown here. In simulations including gravity, the clumps share many characteristics with the observed CO clumps (see Section 3.5) in terms of mean density, velocity dispersion and mass spectrum (*e.g.* Banerjee et al. 2009). The structure of the cloud remains largely unchanged. The salient difference with the non self-gravitating case is that the PDF of the gas density extends towards much larger values (see later discussion of the density PDF). However, the bulk of the mass, though, remains comprised in gas of density in the range $n_{\text{H}} = 100 - 10^3 \text{ cm}^{-3}$, even at late times, when densities as large as 10^6 cm^{-3} are reached.

In a third step, UV-driven chemistry has been introduced either directly during the simulation (*e.g.* Glover & MacLow 2007) or, at a more sophisticated level, as a post-treatment of the WNM colliding flow simulations (*e.g.* Levrier et al. 2012). This allows a proper treatment of the combined influence of density and UV-shielding upon chemistry (see Sect. 6) and of the cooling function. The results provide a confirmation that the gas temperature is reasonably well computed in the magneto-hydrodynamical (MHD) simulations. Levrier et al. (2012) beautifully reproduce the observed behavior of molecules such as CH with column densities of H_2 (*e.g.* Gerin et al. 2010) but, interestingly, fail to reproduce (by almost a factor of 10) the observed CO abundances in regions poorly shielded from the UV-field. Several methods to follow CO formation in turbulent simulations have been compared by Glover & Clark (2012): they find that, not unexpectedly, the gas dynamics is not sensitive to the details of the chemistry models, but all the adopted models so far fail to reproduce the CO abundances in such regions (Shetty et al. 2011).

All these results are quantitatively in good agreement with the two-phase picture of molecular clouds proposed above. They illustrate the importance of the connection between molecular clouds and their surrounding low-density medium. Moreover, they stress the major role of large-scale velocity perturbations (shocks,

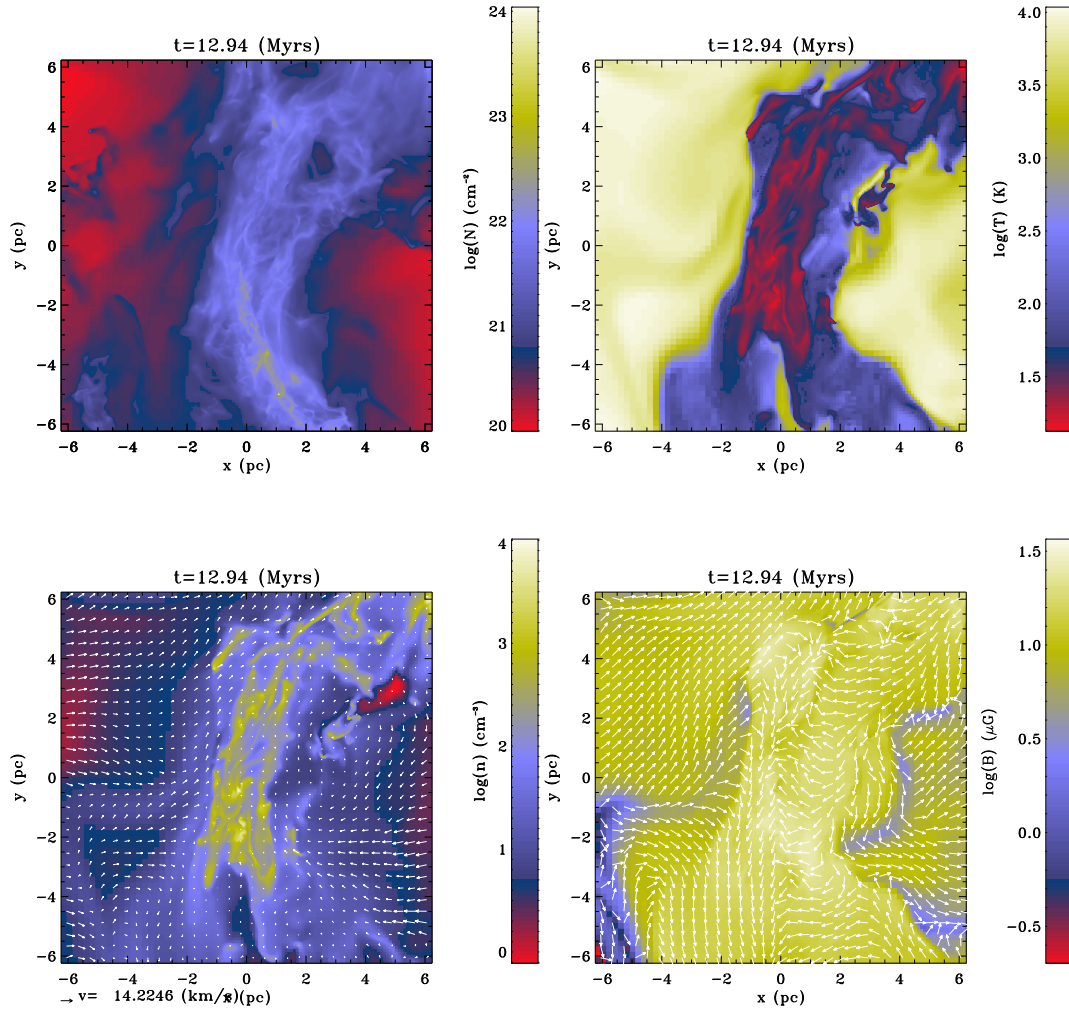


Fig. 3 Column density (*top left*), and cuts of the density with projected velocity field (*bottom left*), temperature (*top right*) and magnetic field (*bottom right*) of a simulation snapshot of molecular cloud formation (Hennebelle et al. 2008). While the total magnetic intensity is shown, the arrows indicate the direction of the field in the XY plane.

turbulence) in the low density gas upon the thermodynamical evolution of the whole medium.

In parallel to these works, which focus on the scale of a single molecular cloud, a series of studies have been conducted to understand the formation of molecular clouds at large scale. A first type of studies (e.g. Vázquez-Semadeni et al. 1995, de Avillez & Breitschwerdt 2005, Joung & Mac Low 2006, Koyama & Ostriker 2009) consider scales of about 1kpc with supernovae explosions as the main driver of interstellar turbulence. The second approach treats a whole galactic disk in-

cluding the gravity of stars either in a fixed asymmetric potential (e.g. Tasker & Tan 2009), or in a prescribed spiral arm potential (e.g. Dobbs & Bonnell 2007) or with self-consistent dynamics of stars (e.g. Bournaud et al. 2010, Hopkins et al. 2011). Not surprisingly, it is found that spiral arms play an active role in triggering molecular cloud and star-formation. These approaches are complementary to those treating the formation of individual clouds since they provide a consistent description of the cloud formation mechanisms. In particular, statistics can be obtained such as the cloud mass spectrum and internal velocity dispersion. Many of these observed properties are satisfactorily reproduced, though the numerical resolution remains limited, suggesting that the origin of molecular clouds is indeed due to the interaction between turbulence and gravity.

3 The turbulent velocity field

The nature and properties of turbulence in the ISM are still a highly debated and controversial issue in spite of dedicated observational and numerical efforts. This is due in part to the huge range of scales separating those of the energy injection (at the Galaxy scale and even beyond when infall is taken into account), from those where it is dissipated, presumably below the milliparsec scale. It is also due to the fact that the turbulence is compressible, magnetized and multi-phase. Unraveling the properties of interstellar turbulence is essential, though, because along with the magnetic fields, it represents the main contributions to the pressure of the ISM in equilibrium in the galactic gravitation potential field and the main support of molecular clouds against their self-gravity. Turbulence dissipation is therefore a key process among those leading to the formation of molecular clouds, star-formation, and therefore Galaxy evolution (see the reviews of Elmegreen & Scalo 2004 and Scalo & Elmegreen 2004, MacLow & Klessen 2004, McKee & Ostriker 2007).

3.1 A few words on incompressible hydrodynamical turbulence

The definition of turbulence is built on experiment. Turbulence is an instability of laminar flows that develops as soon as the inertial $\mathbf{v} \cdot \nabla \mathbf{v}$ forces greatly exceed the viscous $\nu \Delta \mathbf{v}$ forces (ν is the kinematic viscosity), *i.e.* when the Reynolds number $Re = lv_l/\nu$, at a scale l of characteristic velocity v_l , exceeds a few hundreds. This instability at scale l is at the origin of an energy transfer to smaller scales, which eventually become unstable too and transfer their kinetic energy to even smaller scales, etc. This is the turbulent cascade that develops between the integral scale, L , at which energy is injected, and the dissipation scale l_D , close to the particle mean-free-path, where energy is dissipated into heat due to the particle viscosity. The time-scale for the growth of this instability is of the order of the turnover time $\tau_l = l/v_l$ at each length scale l . Kolmogorov (1941) predicted the self-similar behavior of the velocity field in incompressible turbulence by postulating a dissipationless cascade characterized by a transfer rate of kinetic energy independent of scale, $\epsilon \propto v_l^2/\tau_l = v_l^3/l$, hence the well-known scaling $v_l \propto l^{1/3}$. It is easy to demonstrate that this assumption leads to an energy spectrum $E(k) = k^2 P_v(k) \propto k^{-5/3}$ known as the Kolmogorov spectrum. $P_v(k) \propto k^{-11/3}$

is the power spectrum of the velocity. $E(k)$ has the dimension of a kinetic energy per unit mass *and* unit wavenumber because the average specific kinetic energy at scale $l = 2\pi/k$ is $\langle v_l^2 \rangle = \int_k^\infty E(k') dk'$. In Kolmogorov turbulence, the turnover time-scale τ_l therefore decreases towards small scales while the velocity gradient $v_l/l \propto l^{-2/3}$ slowly increases.

3.2 Intermittency of turbulence

For half a century now, turbulence has been recognized to be intermittent, *i.e.* the smaller the scale, the larger the spatio-temporal velocity fluctuations, relative to their average value. Turbulent energy is not evenly distributed in space and time by the turbulent cascade: at each step of the cascade, the active sub-scales do not fill space so that the subset of space on which the active scales are distributed has a multifractal geometry (see the review of Anselmet et al. 2001 and the book by Frisch 1996). The statistical properties of the velocity fluctuations have been widely studied experimentally in laboratory and atmospheric flows: in all cases, the statistics of *velocity derivative and increment* signals are found to be non-Gaussian, with large departures from the average more frequent than for a Gaussian distribution. The PDF of the turbulent velocity field (projections and modulus), in turn, remains Gaussian. Moreover, the departure of the *velocity increments* PDFs from a Gaussian distribution increases as the lag over which the increments are measured decreases. All the functions of the velocity involving a spatial derivative have therefore non-Gaussian PDFs: the velocity gradients ($\partial_i v_i$) and shears ($\partial_j v_i$) and, accordingly, the rate-of-strain $S_{ij} = \partial_j v_i + \partial_i v_j$ and the dissipation rate $\epsilon_D = \frac{\nu}{2} \Sigma_{ij} (\partial_j v_i + \partial_i v_j)^2$, with non-Gaussian wings more pronounced at small scale.

The quantitative signature of intermittency appears in the behavior of the high-order structure functions of the longitudinal velocity field measured over a lag l , $\langle [\delta v_x(l)]^p \rangle \propto l^{\zeta_p}$. This relation is statistical, not deterministic, and the brackets hold for an average over an “appropriate”, (*i.e.* large enough) volume with respect to l^3 . The anomalous scaling of the exponents $\zeta_p \neq p/3$ characterizes the degree of intermittency and provides the multifractal dimension of the most singular structures, *i.e.* that of the subset of space where the smallest active regions, and turbulent dissipation, are distributed (Anselmet et al. 2001). In incompressible turbulence, the so-called *active small scales* are those of largest vorticity or velocity shear.

Various models have been proposed to explain the values of ζ_p (e.g. Frisch 1995). The most successful is certainly that of She & Levêque (1994) who infer the relation

$$\zeta_p = \frac{-\gamma + 1}{3} p + \gamma \frac{1 - \beta^{p/3}}{1 - \beta}, \quad (1)$$

where γ is the exponent of the dissipation rate scaling in regions containing the most intermittent structures and β is related to the codimension C of the most intense dissipation structures as $\gamma/(1 - \beta) = C$. It is now well established that this relation arises from Poisson statistics (Dubrulle 1994, She & Waymire 1995, Pan et al. 2008). The physical underlying idea is that the dissipative rates at two scales are related by a multiplicative factor which is itself the result of dissipative events and

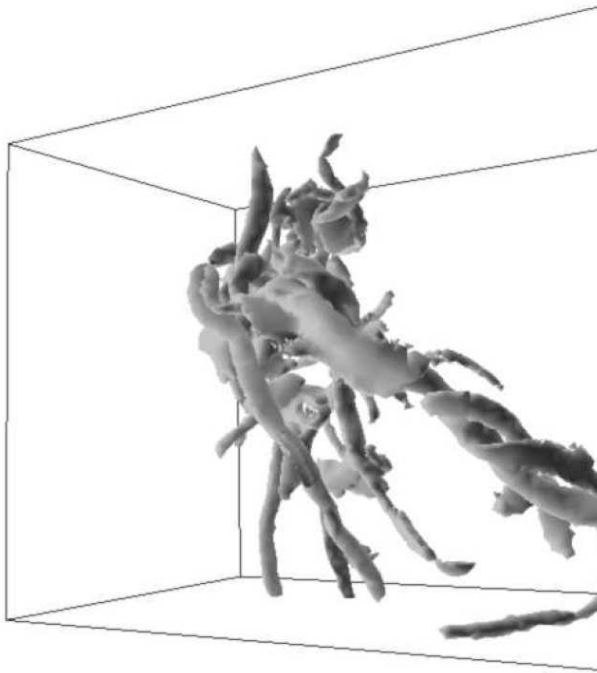


Fig. 4 Structure of most intense vorticity found in numerical simulations of 3-dimensional incompressible hydrodynamical turbulence. The pattern shown, consisting of a large tube surrounded by smaller ones wrapped around it, is frequently found (from Moisy & Jiménez 2004). In MHD turbulence, structures in which turbulent dissipation is concentrated appear to be more sheet-like (Politano & Pouquet 1995).

defects (*i.e.* lack of dissipative events). The latter follows Poisson statistics. For incompressible hydrodynamical turbulence, the most dissipative structures tend to be filamentary so $C = 3 - 1 = 2$ while $\gamma = 2/3$ is assumed.

Anticipating slightly on the next sections, Eq. (1) has been used in the context of supersonic turbulence (Boldyrev et al. 2002) and magnetized turbulence (Politano & Pouquet 1995, Müller & Biskamp 2000). For instance, for supersonic turbulence, it is expected that the dissipative structures are sheets rather than filaments which leads to a codimension $C = 1$ instead of 2 and therefore a parameter $\beta = 1/3$.

Another essential facet of turbulent intermittency is that the active small scales are not randomly distributed in space but are organized into coherent structures – *the sinews of turbulence*, as qualified by Moffatt et al. (1994). In incompressible turbulence, the structures of largest vorticity tend to be filamentary as shown in Fig. 4, while those of highest rate-of-strain and dissipation are rather in the form of sheets or ribbons, following the analysis of numerical simulations by Moisy & Jiménez (2004). These structures are remarkable in the sense that they are both large scale, *i.e.* their length is comparable to the integral scale of turbulence, and small scale structures, *i.e.* they have substructure down to the dissipation scale. The coupling between large scales and small scales operated by turbulence is repeatedly found in simulations. Mininni et al. (2006) find that small-scale

intermittency is more pronounced in turbulent fields where the large-scale shear is larger.

3.3 Incompressible magnetized turbulence

While the simple Kolmogorov dimensional scaling relation, described above, has proven to be very robust, MHD flows appear to be much more difficult to understand. Indeed, despite more than 35 years of analytical, numerical and observational investigations, the energy spectrum of MHD turbulence remains a subject of controversy. The first attempt to establish such a spectrum has been done by Iroshnikov (1963) and Kraichnan (1965). In incompressible MHD turbulence, any function $\mathbf{v} \pm \mathbf{b}(\mathbf{r} \pm \mathbf{v}_A t)$ of \mathbf{v} and \mathbf{b} , the velocity and magnetic field \mathbf{B} fluctuations, is a solution of the MHD equations (here $\mathbf{v}_A = \mathbf{B}/\sqrt{4\pi\rho}$ is the Alfvén velocity). This implies that Alfvén wave packets traveling in the same direction along the magnetic field are not interacting. Thus, the interaction between wavepackets occurs only between wavepackets moving in opposite directions. The collision time t being about $(kv_A)^{-1}$, the change in the velocity δv_l is estimated from the non-linear advection term $\delta v_l/t \simeq v_l^2 k$, so that one gets the fractional change in the velocity, $\delta v_l/v_l$, proportional to v_l/v_A . Consequently, the number of collisions, N , needed for a wavepacket to be significantly modified is $N \simeq (v_A/v_l)^2$. This is because the phase of the wavepacket is changing randomly during a collision. Thus the cascade time is about $\tau \simeq N/(v_A k)$. Assuming that the energy flux is the same at all scale, one gets $v_l^2/\tau \simeq \epsilon$, which leads to $v_l^4 \propto k^{-1}$ from which one infers $v_l \propto l^{1/4}$ and $E(k) = k^2 P_v(k) \propto k^{-3/2}$. The energy spectrum $E(k) \propto k^{-3/2}$ is thus slightly shallower than the Kolmogorov one. An essential assumption of the Iroshnikov–Kraichnan approach is that the eddies are isotropic, *i.e.* have the same spatial extension in the field-parallel and field-perpendicular directions. However, numerical and observational data accumulated for the last 30 years indicate that in MHD turbulence the energy transfer occurs predominantly in the direction perpendicular to the field (Biskamp 2003). This raises the question whether the picture proposed by Iroshnikov and Kraichnan is grasping the essential physical mechanisms.

An important progress has been performed by Goldreich & Sridhar (1995) who have developed a theory which takes into account the anisotropy of the eddies in MHD. They suggested that as the energy cascade proceeds to smaller scales, turbulent eddies progressively become elongated along the large-scale field. More precisely, assuming that the Alfvén time-scale and the non-linear cascade time-scale are in critical balance $k_z v_A \simeq v k_\perp$, and that the cascade time in the perpendicular direction is still leading to $v_\perp \propto k_\perp^{-1/3}$, they infer that the wave vector along the z-axis is related to the wave vector $k_z \propto k_\perp^{2/3}$. As a consequence, they found that the energy transfer time is different from the Iroshnikov–Kraichnan estimate, and identical to the Kolmogorov one. This leads to a scaling for the field-perpendicular energy spectrum, $E(k_\perp) \propto k_\perp^{-5/3}$. More recently, this issue has been investigated further in various analytical and numerical studies (e.g. Cho et al. 2002, Boldyrev 2005, Lee et al. 2010, Beresnyak 2011, Mason et al. 2012, Wan et al. 2012) and still appears to be a matter of debate. Indeed, even the question of the universality of the energy spectrum in incompressible MHD turbulence remains unsolved.

3.4 Supersonic turbulence

In the ISM, turbulence is observed to be highly supersonic with respect to the cold gas. Given the complexity of the problem, it is not surprising that very few results have been rigorously established analytically (see nonetheless the recent work by Galtier & Banerjee 2011 who attempt to obtain a rigorous expression for the two-point correlation function) and most of our understanding comes from numerical simulations performed during the last two decades. The biggest simulation performed to date is that by Kritsuk et al. (2007) with an effective resolution of 2048^3 computing cells. In the one dimensional case (*i.e.* Burgers turbulence, see Bec & Frisch 2000 for a review), one expects the power spectrum of the velocity v to be $P_v(k) \propto k^{-2}$. The reason is that a Fourier transform of an Heavyside function, which is a good representation for shocks, is proportional to k^{-1} . Thus, the energy spectrum is slightly stiffer than the Kolmogorov spectrum. In high resolution 3D numerical simulations, the power spectrum of v is $P_v(k) \propto k^{-3.95}$ (Kritsuk et al. 2007). Thus, in 3D, the velocity power spectrum exponent α is bracketed by that of incompressible Kolmogorov turbulence ($\alpha=11/3=3.67$) and that of Burgers turbulence ($\alpha=4$) which is fully compressible. This is so because even highly supersonic flows tend to have a large energy fraction in the solenoidal (or incompressible) modes (e.g. Porter et al. 2002, Kritsuk et al. 2007, Federrath et al. 2010), in particular when the flow is significantly magnetized (Vestuto et al. 2003).

An interesting issue, explored by Kritsuk et al. (2007) concerns the power spectrum of the density weighted velocity, $\rho^{1/3}v$. This quantity stems from the fact that the energy flux, which for incompressible turbulence is simply $\propto v_l^3/l$, becomes $\rho v_l^3/l$ for compressible fluids. Thus $\rho v_l^3/l \simeq \epsilon$. Interestingly, Kritsuk et al. (2007) find that the power spectrum of this quantity has an exponent much closer to 11/3 than the power spectrum of v . This raises the question as to whether the ideas of Kolmogorov regarding the invariance of the energy transfer rate, can be generalized and applied to compressible flows (see also Galtier & Banerjee 2011). Indeed, observations have provided answers to these questions. We revisit them in the next section.

3.5 Revisited scaling laws and mass spectrum of molecular clouds

Interstellar turbulence has been advocated a long time ago (von Weizsäcker 1951) on the basis of estimated large Reynolds number $Re \gg 10^7$ but formal proofs are hard to gather. The linewidth of a set of molecular clouds in the Galaxy was shown to increase as a power of their size, with a spectral index, $p = 0.38$, reminiscent of the scaling of velocity fluctuations in incompressible turbulence (Larson 1981). This pioneering study has now been extended to a variety of molecular clouds and tracers (Solomon et al. 1987, Falgarone et al. 1992, Heyer & Brunt 2004) and extended to external galaxies. This scaling has been often challenged because it is difficult to recognize it on data samples that have too small a dynamic range. In addition, the scaling laws derived from $^{12}\text{CO}(J=1-0)$ emission differ from those inferred from other tracers (^{13}CO , CS, CN, NH_3 , ...).

CO structures are defined as connected structures identified in the position-velocity space of $^{12}\text{CO}(J=1-0)$ maps. Size, internal velocity dispersion and column

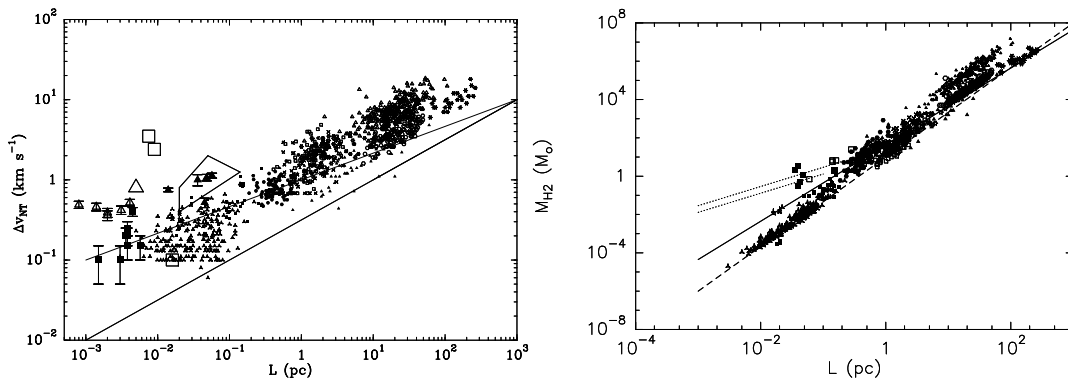


Fig. 5 Scalings of the masses and velocity dispersions with sizes of a large sample of molecular clouds. The cloud properties are inferred from their $^{12}\text{CO}(J=1-0)$ line emission. (*Left*) Non-thermal velocity dispersion versus size scale. The solid lines show the slopes $p = 1/3$ and $1/2$ of the scaling law $\Delta v_{NT} \propto L_{pc}^p$ (see references in Falgarone et al. 2009). (*Right*) Gas mass versus size scale. Different scalings, $\gamma = 2$ (solid line), $\gamma = 2.3$ (dashed line) defined by $M(L) \propto L^\gamma$ are shown. The scaling of isothermal self-gravitating polytropes with size ($\gamma = 1$) is also shown for two gas temperatures 10 K and 20 K (dotted lines). The largest symbols (open and solid squares) refer to low-mass dense cores from the samples of Ladd et al. (1994) and Lada et al. (1997).

density (therefore mass) have been computed for each of these structures. Figure 5 is an illustration of the mass–size and linewidth–size scalings of such CO structures (see references in Falgarone et al. 2004, 2009). The method of structure extraction has long been criticized on the justified basis that similar (or adjacent) projected velocities do not imply actual spatial connection of the structures identified in position–velocity space (Ostriker et al. 2001). However, a similar linewidth–size scaling law has been obtained between 0.05 pc and 20 pc with a different method (Ossenkopf & Mac Low 2002).

Figure 5 prompts four comments: (*i*) the linewidth–size relation has quite a large dispersion (about a factor of 10) about $\Delta v_{NT} \sim 1 \text{ km s}^{-1} L_{pc}^{0.5}$. (*ii*) There is even a larger scatter (a factor of 50–100) below 0.1 pc: the data points correspond to the small-scale structures of Heithausen (2002, 2004, 2006), Sakamoto & Sunada (2003) and Falgarone et al. (2009). (*iii*) When drawn over almost five orders of magnitude in size scale, as in Fig. 5, the mass–size scaling law cannot be restricted to one single scaling $M(L) \propto L^\gamma$. Values between $\gamma = 2$ (solid line) at large scales and $\gamma \sim 2.3$ (dashed line) at scales smaller than ~ 0.5 pc may be more relevant. Note that using clouds extracted from the $^{13}\text{CO}(1-0)$ Galaxy Ring Survey, Roman-Duval et al. (2010) find a single (and very accurate) scaling with $\gamma = 2.36 \pm 0.04$. The range of size scales involved is only 0.7 – 30 pc, which shows the sensitivity of such slope determinations to the sample dynamic coverage. (*iv*) At scales smaller than ~ 0.5 pc, the mass in a given size scale varies by orders of magnitude between self-gravitating dense cores and much less massive structures of the same size. Therefore there is no such density–size scaling law $\rho \propto L^{-1}$ that would be relevant to all small scale structures, as already noted by Falgarone et al. (1992).

The linewidth–size (LWS) relation has often been used to argue that molecular clouds are in virial balance between internal energy and self-gravity, with their mass M , radius $R = L/2$ and 1-dimensional internal velocity dispersion σ related

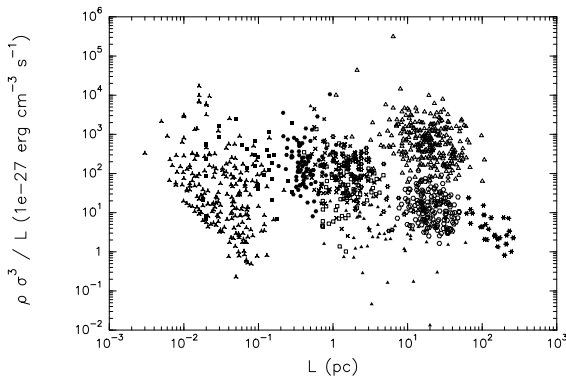


Fig. 6 Kinetic energy transfer rate $\rho\sigma^3/L$ versus size scale. Note that the value of this rate inferred from HI in the Solar Neighborhood is $\sim 10^{-25}$ erg cm $^{-3}$ s $^{-1}$ (see Table 1).

by $5\sigma^2 = GM/R$, where the geometric factor holds for spherical clouds (Bertoldi & McKee 1992). In this virialized LWS relation, the coefficient between the linewidth and the size depends on the cloud mass (or surface density $\Sigma = M/\pi R^2$) so that $\sigma/R^{1/2} \propto \Sigma^{1/2}$ (McKee, Li & Klein, 2010). Falgarone & McKee (2013, in preparation) show that molecular clouds traced by ^{12}CO in the Galaxy are virialized only above a surface density threshold $\Sigma \sim 100 \text{ M}_\odot \text{ pc}^{-2}$. The GMCs, as traced by CO, are virialized *and* follow the same LWS relation as lower mass clouds: below this threshold, the internal velocity dispersion (and its large scatter) is independent of Σ , $\sigma \propto R^{1/2}$, and this LWS relation may be interpreted as a manifestation of the turbulent nature of the cloud internal motions. In their analysis of the Galactic Ring survey in $^{13}\text{CO}(1-0)$ emission, Heyer et al. (2009) find that $\sigma/R^{1/2} \propto \Sigma^{1/2}$, and that the molecular clouds sampled by this survey are in virial balance. As a consequence, they rule out the interpretation linked to turbulent scaling laws. Since $^{13}\text{CO}(1-0)$ line is more optically thin than the $^{12}\text{CO}(1-0)$ transition, the survey does not probe surface densities as low as $\sim 1 \text{ M}_\odot \text{ pc}^{-2}$, which ^{12}CO emission does, and the change of behavior at $\Sigma \sim 100 \text{ M}_\odot \text{ pc}^{-2}$ has been missed because of the intrinsic scatter of the data points. The same limitation appears to apply to the discussion of Field et al. (2011) that relies on this data set.

The two different LWS relations may be reconciled with a more general expression of the virial theorem that takes surface terms (or an external pressure) into account:

$$\ddot{I} = 2M\mathcal{E} - \gamma GM^2/R - 4\pi P_{ext}R^3 = 0, \quad (2)$$

where $\mathcal{E} \propto \sigma^2$ is the specific internal energy due to turbulence and $\gamma \sim 1$ depends on the degree of the gas concentration at each scale. Keto & Myers (1986) had already found that diffuse clouds are not gravitationally bound and interpreted the departure of $\sigma/R^{1/2}$ from the $\Sigma^{1/2}$ dependence as the cloud being in quasi-static equilibrium with an intercloud medium exerting a confining pressure $P_{ext}/k \approx 10^{3.5}-10^{4.5}$ K cm $^{-3}$. From the above virial balance equation, in the regime of non-gravitationally bound clouds, $\sigma/R^{1/2}$ scales as $\Sigma^{-1/2}$, a behavior absent in the $^{12}\text{CO}(1-0)$ data set.

The independence of σ^2/R on Σ is obtained if P_{ext} and Σ have the same scaling with size. Indeed, this is what is found in the above $^{12}\text{CO}(1-0)$ cloud sample where

the kinetic pressure increases with scale as $\frac{1}{2}\rho\sigma^2 \sim 10^{-11}R_{pc}^\delta \text{ erg cm}^{-3}$, with $\delta \sim 0.25 - 0.5$. If this non uniform pressure acts as a confining pressure, then at each scale, $P_{ext} \propto R^\delta$ which is close to the scaling $\Sigma \propto R^{0.3}$ inferred from the observed $M \propto R^{2.3}$. Thus, we would have P_{ext}/Σ being nearly constant as suggested by $\sigma \propto R^{1/2}$. The exact meaning of this relation remains however a little elusive since σ^2 certainly contributes to the internal pressure as well.

This scenario is reminiscent of the hierarchy of clouds in dynamical equilibrium at all scales, with $P_{ext} = \Pi(R)$, as proposed by Chièze (1987). However, one has to understand why the turbulent pressure, at each scale, would act as an *isotropic* stabilizing factor (as it is in the case of isothermal self-gravitation polytropes bound by an external thermal pressure). Chièze (1987) ended his paper by asking what is the physical nature of the process which tends to maintain a constant energy density in molecular matter over a wide range of linear scales. We now know that $\Pi(R)$ is not exactly constant, and that the process that controls the energy density across the scales is called turbulence.

These results shed light on the question “What shapes the structure of molecular clouds: turbulence or gravity?” (Field et al. 2008, 2011, Kritsuk & Norman 2011). As these latter authors show, the scaling laws can, to a large extent, be interpreted as a signature of supersonic turbulence. The above discussion suggests however that gravity certainly modifies the picture. The gas surface density threshold above which clouds are in virial balance between self-gravity and internal energy is comparable to the stellar surface density within 1 kpc of the Sun, $\sim 90 \text{ M}_\odot \text{ pc}^{-2}$, and one order of magnitude larger than that of the gas, on average, $\Sigma_{gas} \sim 10 \text{ M}_\odot \text{ pc}^{-2}$. In their numerical simulations, Koyama & Ostriker (2009) find that the mass-weighted midplane mean pressure is about one order of magnitude larger than that of the midplane mean gas pressure. They argue that self-gravity concentrates gas and increases the pressure within molecular clouds without raising the ambient pressure. They also show that the correlation of the molecular gas fraction with the midplane pressure observed in external galaxies by Blitz & Rosolowsky (2004, 2006) is retrieved only if the epicyclic frequency κ and Σ are kept proportional. This fact introduces galactic rotation as an additional parameters driving the evolution of molecular clouds, a picture which has started to emerge from recent observations (Swinbank et al. 2010, Herrera et al. 2011, 2012).

Last, the kinetic energy transfer rate $2\epsilon = \rho\sigma^3/L$ is displayed as a function of the size in Fig. 6. It is remarkable that the kinetic energy transfer rate in the whole population of molecular clouds traced by ^{12}CO shows no trend of variation from structures of $\simeq 0.01 \text{ pc}$ to GMCs of $\simeq 100 \text{ pc}$ (the same large scatter of ϵ is observed at all scales) and has the value observed in the HI gas (see Table 1). Although the dispersion of ϵ is large at each scale, this result suggests that ϵ is indeed an invariant of the hierarchy of *molecular clouds traced by $^{12}\text{CO}(1-0)$* and that these clouds are part of the same turbulent cascade as the atomic ISM. This conclusion is in remarkable agreement with Kritsuk et al. (2007), generalizing the ideas of Kolmogorov to compressible turbulence.

The same methods used to isolate connected CO structures in space-velocity space allow the construction of mass spectra, $dN/dM \propto M^{-\alpha}$. Different samples provide very close exponents: $\alpha = 1.83$ for $10^3 \text{ M}_\odot < M < 2 \times 10^6 \text{ M}_\odot$ in the early CO survey of the inner galactic plane (Solomon et al. 1987), $\alpha = 1.80$ for $500 \text{ M}_\odot < M < 10^6 \text{ M}_\odot$ from the CO survey of the outer galaxy (Heyer et al. 2001)

Table 1 Characteristics of the turbulence observed in various components of the ISM (Solar Neighborhood). ϵ is expressed in L_{\odot}/M_{\odot} for comparison with the energy provided by stellar radiation, $\frac{1}{2}\bar{\rho}v_l^3/l$ in $\text{erg cm}^{-3} \text{ s}^{-1}$ and P_{turb} in erg cm^{-3} .

	CNM+WNM	molecular clouds	low-mass dense cores
$\bar{n}(\text{cm}^{-3})$	30	200	10^4
l (pc)	10	3	0.1
σ_l (km s^{-1})	≈ 3.5	1	0.1
B (μG)	10	20	100
v_A (km s^{-1})	3.4	2	1.4
$\epsilon = \frac{1}{2}v_l^3/l$	10^{-3}	10^{-4}	10^{-6}
$\frac{1}{2}\bar{\rho}v_l^3/l$	2×10^{-25}	1.7×10^{-25}	2.5×10^{-25}
$P_{turb} = \frac{1}{3}\bar{\rho}v_l^2$	3×10^{-11}	2×10^{-11}	10^{-11}

and $\alpha = 1.84$ over $10^{-3}M_{\odot} < M < 50M_{\odot}$ in a high latitude cloud (Heithausen et al. 1998). The slopes of the mass spectra *of structures identified from CO lines* are therefore found to be the same over nine orders of magnitude in masses, in the inner and outer Galaxy, in GMCs and cirrus clouds, in star forming and in inactive regions. Similar values, with larger error bars, have been found in a number of smaller samples covering the mass range 10 to $10^3 M_{\odot}$.

3.6 Source of turbulent energy in molecular clouds

A longstanding issue is the origin of the observed turbulent velocity dispersion of molecular clouds. Indeed, turbulent supersonic motions are expected to rapidly dissipate in shocks within a cloud crossing time, ≈ 1 Myr, for clouds of a few pc and internal velocity dispersion of a few km s^{-1} . This has been largely confirmed by numerical simulations (e.g. MacLow 1999, MacLow & Klessen 2004) which have demonstrated, despite early speculations, that the magnetic field is not changing this result significantly, *i.e.* in a few crossing times most of the energy has decayed. Since turbulent energy is decaying fast and that molecular clouds remain turbulent, turbulence has to be continuously replenished. The question is how.

Again, observations are providing clues to this question. First, turbulence in molecular clouds that are not forming stars, as for instance the Maddalena cloud, is comparable to that in more actively star forming clouds (Williams et al. 1994). This is also found by Kawamura et al. (2009) in the LMC: the velocity dispersions they report for two categories (*i.e.* clouds without and with massive stars) are very similar (*e.g.* their Table 4). Second, there is no evidence for a characteristic scale in the velocity field. Ossenkopf & MacLow (2002) using various methods conclude that it is consistent with a forcing at a scale larger or equal to the size of the clouds they study. This is also found by Brunt et al. (2009), who confront synthetic molecular lines to real observations. This suggests that, at least for a large fraction of clouds, the turbulent driving is external, *i.e.* most of the energy is injected from outside.

Klessen & Hennebelle (2010) argue that turbulence is driven by accretion onto the molecular clouds. Indeed when a piece of fluid falls onto the cloud, it carries a certain amount of kinetic energy which can be used to sustain turbulence in the molecular cloud. The question is then whether the energy injection rate, $\dot{E}_{in} \simeq S_c \times v_{in} \times \frac{1}{2}\rho_{in}v_{in}^2$, where S_c is the cloud surface, v_{in} is the infall velocity

of the gas and ρ_{in} its density, can compensate for the turbulent dissipation rate $\dot{E}_{dis} \simeq \frac{1}{2}M_c\sigma_c^2/\tau_c \simeq \frac{1}{2\sqrt{3}}M_c\sigma_c^3/L_c$ where M_c , L_c and σ_c are the cloud mass, size and velocity dispersion. The difficulty to perform such an estimate is obviously the lack of empirical knowledge on the accretion rate. From their data Fukui et al. (2009) infer a rate on the order of a few $10^{-2} M_{\odot} \text{ yr}^{-1}$ for typical GMCs, which is enough to reproduce the observed velocity dispersion according to Klessen & Hennebelle (2010). A direct estimate using colliding flow simulations leads to a similar conclusion. Goldbaum et al. (2011) have performed a time-dependent analytical calculation of a molecular cloud evolution and conclude that turbulence can efficiently be driven by accretion. The accretion-driven turbulence model implies that energy is injected in the ISM at large scales in the Galaxy, presumably by a combination of supernovae/bubble expansion and galactic differential rotation, and *cascades* to smaller scales as the gas accumulates into the GMC. This mechanism emphasizes the link between molecular clouds and their environment as described earlier in the review.

When enough stars have formed inside molecular clouds, stellar feedback presumably becomes important. Matzner (2002) computes the impact of stellar winds, supernovae and HII regions onto cloud turbulence and find that HII regions are the most efficient to sustain turbulence. Following Williams & McKee (1997), Matzner concludes that the photo-evaporation induced by the HII regions eventually destroys the cloud. Numerical simulations of the impact of the ionizing radiation from O stars have been performed by Gritschneider et al. (2009, see also Tremblin et al. 2012). They find that it can induce the formation of pillars of dense gas and inject turbulence within molecular clouds. The inclusion of the feedback from protostellar jets has been considered by Nakamura & Li (2007) and Wang et al. (2010). These simulations suggest that protostellar jets can efficiently trigger turbulence at the scale of a stellar cluster (say at a scale of about 1 pc) once enough stars have formed. On the other hand, Maury et al. (2010) estimate the support that the observed protostellar outflows are providing to the star forming clump NGC2264-c and find that it is not sufficient to resist gravitational collapse.

These qualitative estimates show how uncertain the energy injection budget within molecular clouds is. One does not know either when the internal feedback becomes dominant over the external feeding. In their analytical model, Goldbaum et al. (2011) estimate that the total contribution of external and internal sources is roughly comparable over the cloud life time but their model is hampered by large uncertainties.

3.7 Signatures of the intermittency of turbulence in molecular clouds

3.7.1 Parsec-scale coherent structures of intense velocity-shear

Identifying regions of intermittency in interstellar turbulence is challenging for several independent reasons. First, these regions are non-space filling and correspond to rare events in time and space: finding them requires the analysis of large homogeneous statistical samples of the velocity field. This means observations at high spectral and spatial resolution of large interstellar regions unperturbed by star-formation. Second, observations do not provide the full velocity field but only its line-of-sight (*los*) projection provided by the Doppler-shift of a molecular

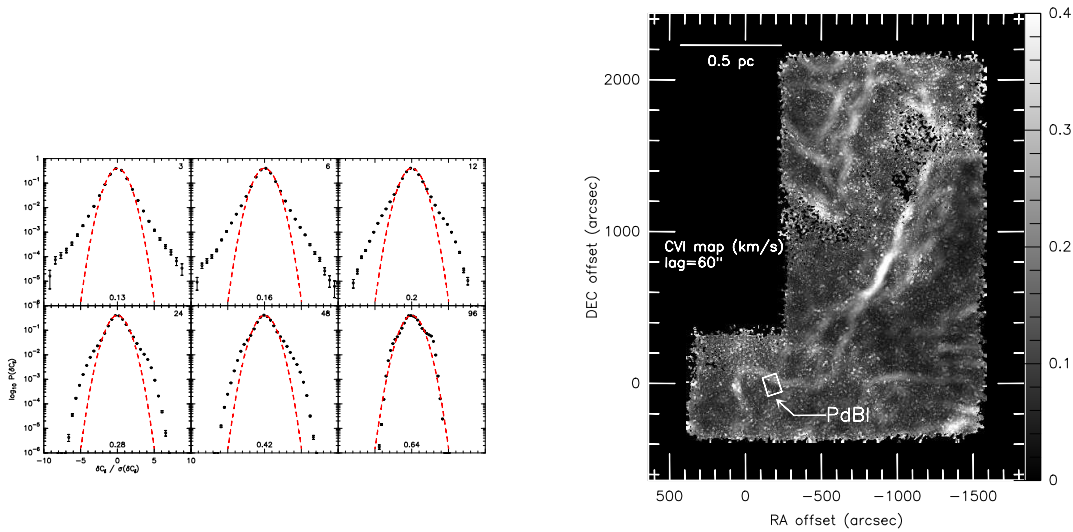


Fig. 7 **Left:** Normalized PDFs of line centroid velocity increments (CVI) measured over variable lags, expressed in units of 15 arcsec (upper right corners), and computed within the field of Fig. 6. The Gaussian of the same dispersion $\sigma(\delta C_l)$ (given in km s^{-1} at the bottom of each panel) are also drawn. The non-Gaussian wings of the PDFs increase as the lag decreases. **Right:** In the same field, locus of the positions populating the non-Gaussian wings of the PDF for a lag of 60 arcsec. The wedge is in km s^{-1} . The rectangle is the area observed with the IRAM-PdBI (From Hily-Blant et al. 2008).

line. Then, statistical analyses similar to those performed in laboratory flows or in the solar wind are not possible. Third, only spatial variations of the los velocity in the plane-of-the-sky (pos) are provided by observations. Therefore, the velocity variations are by essence cross-variations $\partial_j v_i$, *i.e.* velocity shears. Finally, the line emission being integrated along a los , the velocity information at a given position is the full line profile and its moments, the first moment being the line centroid velocity. The statistics of the velocity increments are built using the line centroid velocity increments (CVI) measured between two positions separated by a lag l in the pos (e.g. Lis et al. 1996). The ^{12}CO lines have turned out to be a most useful tool for this search because their large optical depth makes them sensitive tracers of rare events, in particular of the gas that emits at velocities in the far line-wings (*i.e.* extreme dynamic events).

The most recent maps carried out at the IRAM-30m telescope in the $^{12}\text{CO}(2-1)$ line, produce up to $\sim 10^5$ independent spectra homogeneously sampling turbulence in the diffuse molecular gas (Hily-Blant & Falgarone 2009). The CVI-PDFs in that field have the anticipated non-Gaussian wings that increase as the lag over which the increment is measured decreases (Fig. 7, left). The locus of the extreme CVIs (the E-CVIs) that contribute the non-Gaussian wings of the PDFs is an ensemble of elongated narrow structures (~ 0.03 pc thick) (Fig. 7, right). As expected, the lane of largest E-CVIs coincides with the region where the velocity-shears are the largest, $40 \text{ km s}^{-1} \text{ pc}^{-1}$ (Hily-Blant & Falgarone 2009). Most interestingly, it also

coincides with a lane of weak $^{12}\text{CO}(2-1)$ emission and one of the weakest filaments of dust thermal emission detected at $250\mu\text{m}$ in that field with Herschel/SPIRE (see Section 4). Last, two low-mass dense cores in the field lie at the South-East tip of the E-CVIs locus (Heithausen et al. 2002), suggesting a *causal link* between intense turbulent dissipation, the formation of CO molecule, the formation of tenuous dense filaments and, eventually, that of low-mass dense cores.

A similar analysis has been performed in a less turbulent field (specific kinetic energy four times smaller at the parsec-scale) with the same total hydrogen column density as that in the Polaris Flare. The CVI-PDFs show departures from a Gaussian distribution with an amplitude 2.5 times smaller than in the Polaris Flare (Hily-Blant et al. 2008), in agreement with the theoretical predictions of Mininni et al. (2006), *i.e.* the enstrophy density at small scales increases with the amplitude of the large-scale shear feeding turbulence.

This ensemble of properties, *(i)* the increasing departure of CVI-PDFs from a Gaussian distribution as the lag decreases; *(ii)* the spatial coherence of E-CVIs structures and *(iii)* the link between the large-scale properties of turbulence and the magnitude of the small-scale E-CVIs, suggests that the $^{12}\text{CO}(2-1)$ E-CVIs trace the intermittency of turbulence in diffuse molecular clouds. Intermittency is also probed by the non-linear dependence of ζ_p with p up to $p = 6$ discussed in Hily-Blant et al. (2008), a dependence now confirmed, up to higher orders, by the analysis of this larger data set. Unexpectedly (because these exponents are computed on projected velocities), the ζ_p dependence with p in that field agrees, within the error bars, with the She & Levêque (1994) predictions for incompressible turbulence.

3.7.2 Milliparsec-scale observations: approaching the dissipation scales

A step further towards small-scales is provided by the IRAM Plateau de Bure Interferometer (IRAM-PdBI) $^{12}\text{CO}(1-0)$ line observations of the field shown in Fig. 7 (right) at a resolution of ~ 4 arcsec or 3 milli-pc (Falgarone et al. 2009). These observations are unique so far because the lines detected are very weak. The spatial dynamic range of the map is large enough to allow the detection of 8 elongated structures with thickness as small as ≈ 3 milli-pc (600 AU) and length up to 70 milli-pc. These are *not filaments* but appear to be the sharp edges of extended CO emission. Six, out of eight filaments, form pairs of quasi-parallel structures at different velocities. Velocity-shears estimated for the three pairs include the largest values ever measured in non-star-forming regions, up to $780 \text{ kms}^{-1} \text{ pc}^{-1}$. Finally, the PdBI-structures are almost straight and their different position angles cover the same broad range of values as the projection of the magnetic field inferred from absorption towards field stars in that area. This suggests an interesting alignment of the *pos* projections of magnetic fields and velocity shear-layers in these structures. In Section 6, we discuss the new routes that the intermittency of interstellar turbulence opens for molecule formation.

3.8 Anisotropy of turbulence

The presence of large-scale pervasive magnetic fields in the galactic ISM is anticipated to induce anisotropy in the turbulence of molecular clouds. Such an

anisotropy has been sought in a field of the Taurus molecular cloud where polarization of starlight reveals aligned and ordered magnetic fields, associated with strong striations parallel to the field in the $^{12}\text{CO}(1-0)$ emission (Heyer et al. 2008). These authors develop an axis-constrained Principal Component Analysis method that has been tested against numerical simulations of MHD turbulence. In the real data, in spite of projection effects that would tend to reduce it, Heyer et al. find an anisotropy: there is more power at small scales in the spectrum of velocity fluctuations in the direction perpendicular to the striations rather than along them. Interestingly, Heyer & Brunt (2012) have extended this analysis to the whole Taurus molecular cloud finding that the velocity anisotropy is limited to the cloud edges and absent in the opaque regions of large column density. The authors argue that these results, compared to MHD simulations, suggest sub-Alfvénic turbulence in the edges and opposite in the opaque regions.

4 Density structure

In the context of structure formation, the density distribution within molecular clouds must be regarded as a fundamental quantity. In this section we review our knowledge and understanding of the origin of the density distribution.

4.1 The density distribution within molecular clouds

A number of processes can shape the density field of a compressible flow. In the ISM compressible turbulence and gravity are likely to be largely responsible for the gas density distribution. Other important aspects are the equation of state that describes how pressure and density are related as well as the forcing of the turbulence, *i.e.* the way by which the turbulent energy is maintained, which determines the relative importance of solenoidal and compressive modes and not surprisingly turns out to have a significant impact on the density distribution. The dissipation of turbulence may also drive density fluctuations by triggering chemistry, modifying in turn the cooling rates and the equation of state (see Section 6).

4.1.1 The role of supersonic isothermal turbulence

As isothermal supersonic turbulence constitutes a simplified and natural framework, most of the studies have been performed under this assumption. Since the pioneering works of Vázquez-Semadeni (1994, see also Blaisdell et al. 1993) and Padoan et al. (1997), various simulations of hydrodynamic supersonic turbulence, have established that the density PDF is well represented by a log-normal form (e.g. Kritsuk et al. 2007, Federrath et al. 2008, 2010),

$$\mathcal{P}(\delta) = \frac{1}{\sqrt{2\pi\sigma_0^2}} \exp\left(-\frac{(\delta - \bar{\delta})^2}{2\sigma_0^2}\right), \quad \delta = \ln(\rho/\rho_0), \quad (3)$$

$$\bar{\delta} = -\sigma_0^2/2, \quad \sigma_0^2 = \ln(1 + b^2\mathcal{M}^2),$$

where \mathcal{M} is the Mach number, ρ_0 is the mean density and $b \simeq 0.5 - 1$.

An exact derivation of the density PDF is still pending but qualitatively, at least, the origin of this distribution can be understood as a consequence of the fluid particles being repetitively and randomly compressed by the turbulent velocity fluctuations. The key is that density enhancement is a multiplicative process. To illustrate this better, let us consider a fluid particle of density ρ_0 which is compressed by a first shock at mach number \mathcal{M}_1 . The density is then multiplied by \mathcal{M}_1^2 and becomes $\rho_1 = \rho_0 \times \mathcal{M}_1^2$. Then the same fluid particle is compressed by another shock which brings its density to $\rho_2 = \rho_1 \times \mathcal{M}_2^2 = \rho_0 \times \mathcal{M}_1^2 \mathcal{M}_2^2$, hence the density is *multiplied* each time a new shock is passing. A complementary point of view is obtained by considering the quantity $\ln(\mathcal{M}_i^2)$ which is *added* to the logarithm of the density. By virtue of the central limit theorem, one can expect that the distribution of $\ln(\rho)$ must be a Gaussian and therefore that the density must have a log-normal distribution. This argument is the essence of the explanation provided by Kevlahan & Pudritz (2009) and constitutes a nice qualitative explanation. However, it is no more than qualitative for various reasons. First, as shown in Kevlahan & Pudritz (2009), the result depends on the number of shocks which implies that the average number of shocks should be determined. Moreover, this approach does not take into account the reexpansion of the compressed layer between the shocks. Second, as demonstrated by Federrath et al. (2008, 2010), the density PDF is really close to a log-normal only when the forcing is solenoidal, i.e. when the force used to stir the turbulence contains only incompressible modes. When this is not the case, Federrath et al. (2008) show that the density PDF presents significant deviation from a log-normal distribution, in particular at high density.

Beyond the exact shape of the PDF, the dependences of $\bar{\delta}$ and σ_0 given in Eq. (3) are also interesting. The expression of the former is a simple consequence of mass conservation, $\int_{-\infty}^{\infty} \exp(\delta) \mathcal{P}(\delta) d\delta = 1$ from which it is easy to show that $\bar{\delta} = \int_{-\infty}^{\infty} \delta \mathcal{P}(\delta) d\delta = -\sigma_0^2/2$. The dependence of σ_0 on \mathcal{M} is more empirical. The underlying physical idea (Padoan et al. 1997) is simply that the density fluctuation induced by a shock is $\delta\rho/\rho_0 = (\rho - \rho_0)/\rho_0 \simeq b^2 \mathcal{M}^2$, while the variance of the density field, σ_ρ is by definition: $\sigma_\rho^2 = \int (\rho - \rho_0)^2 \mathcal{P}(\rho) d\rho$. However, the high density regions are compressed and occupy a volume fraction $\propto \mathcal{M}^{-2}$. Thus from a spatial integration of the density variance, $\sigma_\rho^2 = (\int (\rho - \rho_0)^2 dV)/\bar{V}$, it is inferred that $\sigma_\rho^2 \propto \mathcal{M}^4/\mathcal{M}^2$. Thus, σ_ρ has a linear dependence on the mach number, $\sigma_\rho \simeq b\mathcal{M}$. Next, as pointed out by Federrath et al. (2008), with a density probability distribution as stated by Eq. (3), it is an easy task to show that $\sigma_0^2 = \ln(1 + \sigma_\rho^2/\rho_0^2)$, by simply writing $\sigma_\rho^2 = \rho_0^2 \int (\exp(\delta) - 1)^2 \mathcal{P}(\delta) d\delta$.

Federrath et al. (2008) propose an heuristic model for the parameter $b = 1 - 2\zeta/3$, where ζ controls the importance of solenoidal and compressible modes. For $\zeta = 1$, the modes are purely solenoidal while they are purely compressible for $\zeta = 0$. For $\zeta = 0.5$, the power in compressible modes is half of the power in solenoidal modes which corresponds to energy equipartition between the modes (see Federrath et al. 2010, Eq. 9). A comparison between a set of numerical simulations and this approach shows a good agreement. As the Mach number increases, the width of the PDF increases. This is because the shocks are stronger and generate larger density contrasts.

4.1.2 Influence of non-isothermal equation of state

When the gas is non-isothermal, the density PDF is not log-normal anymore. Passot & Vázquez-Semadeni (1998) performed 1D simulations for various values of γ . In particular, they found that for $\gamma < 1$ at high densities, the distribution becomes a power-law whose slope index varies with γ . For $\gamma = 0.5$, which is not too far from the value $\gamma = 0.7$ typical for densities of the order of $10^2 - 10^4 \text{ cm}^{-3}$, they infer an index of about -1.2. Audit & Hennebelle (2010) have presented 3D high resolution simulations of colliding flows in the isothermal case and also in the polytropic case, $\gamma = 0.7$. They confirm the power-law behaviour found in 1D by Passot & Vázquez-Semadeni (1998).

The two-phase case has also been investigated by various teams (e.g. Vázquez-Semadeni et al. 2006, Gazol et al. 2005, Audit & Hennebelle 2010). It has generally been found that the density PDF presents two peaks, one at low density (a few particle per cm^{-3}) and one at high density (a few hundreds of particle per cm^{-3}). The thermally unstable region which is continuously filled by the turbulent motions comprises relatively less mass than in the vicinity of the two branches of equilibria. Note that it appears particularly difficult to obtain numerical convergence at high densities (10^3 cm^{-3} and above) for this type of simulations. For example, Hennebelle & Audit (2007) warn that numerical convergence was probably not reached even in their bidimensional $10^4 \times 10^4$ cell simulations.

The influence of the magnetic field on the density PDF has also been investigated by various authors both in the isothermal case (Ostriker et al. 2001, Lemaster & Stone 2008, Molina et al. 2012) and in the two-phase case (e.g. Hennebelle et al. 2008) generally concluding that it has a weak impact. As discussed below, this conclusion accords well with the fact that the gas which is not self-gravitating essentially flows along the field lines.

4.1.3 The role of gravity

As gravity leads to collapse it is clear that it must have a strong impact on the density PDF. Numerical simulations indeed have revealed that as gravity takes over, a high density tail develops precisely because some gas is collapsing (e.g. Klessen 2000, Slyz et al. 2005, Hennebelle et al. 2008, Kritsuk et al. 2011). Moreover it has been found that this tail is typically a power-law with an exponent of about -3/2 (Kritsuk et al. 2011). The latter is interpreted as a consequence of the $\rho(r) \propto r^{-2}$ profile developed by a collapsing sphere (e.g. Shu 1977). Indeed, the volume of the gas whose density lies between ρ and $\rho + \delta\rho$, is $4\pi r^2 dr$. The exponent simply follows from $r \propto \rho^{-1/2}$, $dV \propto \rho^{-3/2} d \log \rho$.

This gravitational tail of the density PDF develops with time. It first affects only the highest density part of the PDF and then becomes gradually important at smaller densities as collapse proceeds.

4.1.4 Observed column density distribution

The density field cannot be directly inferred from observations. Owing to the integration along the line of sight, column densities are usually obtained. Column density PDF within molecular clouds have been observed for the first time by Kainulainen et al. (2009) who determined the extinction from the 2MASS archive

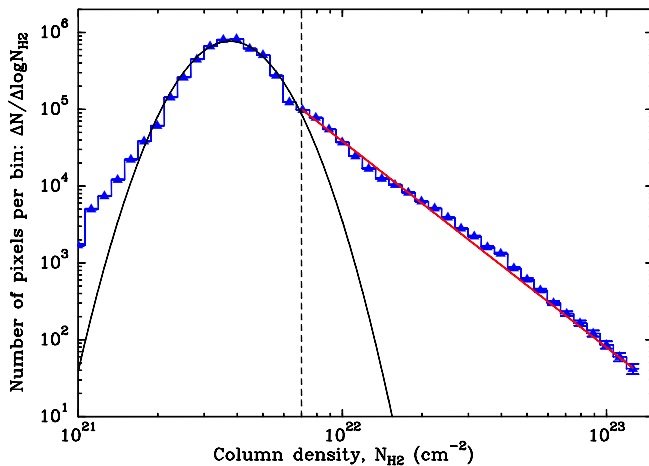


Fig. 8 Column density PDF of filaments in the Aquila star-forming molecular cloud (André et al 2011). The N_{H} values are inferred from the submillimeter dust emission measured by *Herschel*/SPIRE. Note the log-normal and power-law parts. The vertical dashed line marks the extinction that separates the two regimes at visual extinction, $A_V = 3.9$.

and more recently by André et al. (2011) using the thermal dust emission (see Fig. 8). Kainulainen et al. (2009) obtain the column density of 23 nearby molecular clouds. They find that the clouds which are not forming stars, have a log-normal distribution up to extinctions comparable to, or slightly below the cloud mean value. The clouds that are forming stars have also a log-normal distribution but only up to some extinction above which the PDF is more compatible with a power-law and resembles, even quantitatively, the high column density tail found in numerical simulations (see Fig. 9 from Kritsuk et al. 2011). As shown by Kritsuk et al. (2011), this result can be understood by the following argument. In projection the surface of a sphere lying between radius r and $r+dr$ is $dS \propto r dr$. Assuming that the density is proportional to r^{-2} , the column density $\Sigma \simeq r\rho$ is thus proportional to r^{-1} and thus $dr \propto d\Sigma/\Sigma^2$. Thus, we get $dS \propto \Sigma^{-2} d \log \Sigma$.

Turbulence, however, is not the unique explanation for having a log-normal PDF as argued by Tassis et al. (2010). Therefore, it should not be used as a direct proof in favor of the existence of supersonic turbulence but as a fact compatible with it. Finally, we note that in some cases, at low visual extinction, the PDF deviates significantly from the log-normal distribution (see Fig. 8) and appears to be reminiscent of the column density inferred in two-phase flows (e.g. Hennebelle et al. 2008).

4.2 Density higher order statistics

Beside the density PDF, which does not entail spatial correlations in the flow, higher order statistics have been investigated both in simulations and observations.

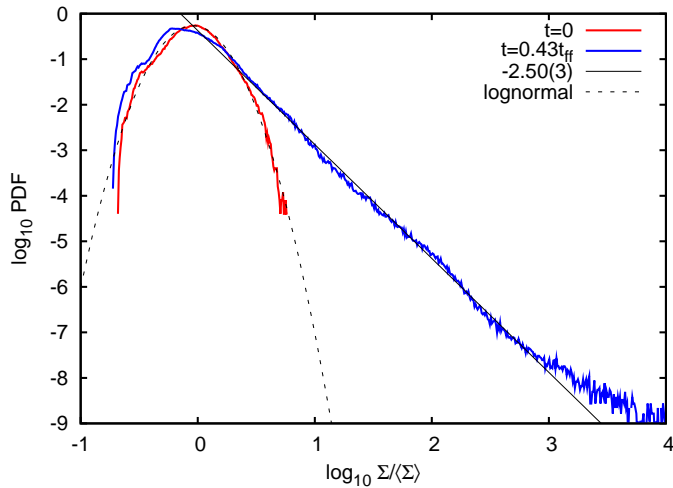


Fig. 9 Column density PDF within the simulation by Kritsuk et al. (2011). At $t = 0$ the distribution is log-normal. At later times, a high density power-law tail develops.

4.2.1 Density power spectra: theory

One of the most fundamental quantity in turbulence is the power spectrum, which, in the case of the velocity field, describes how energy is distributed and a lot of effort has been made to infer the power spectrum of the density field.

In the limit of weakly compressible flows, analytical expansions have been performed by Zank & Matthaeus (1990) and Bayly et al. (1992). They conclude that the result is not universal and depends on the thermal properties of the flow. When the pressure, density and temperature fluctuations are all of the same order, they predict that density should behave like pressure and the power spectrum should be proportional to $P_\rho(k)k^2 \propto k^{-7/3}$. On the other hand, when the temperature and density fluctuations are large with respect to the pressure ones, the density is close to a passive scalar which in turn implies that the power spectrum should be $P_\rho(k)k^2 \propto k^{-5/3}$. Note that it is necessary to go through their analytical expansions to reproduce these results. As molecular clouds are very compressible, it is unclear that these analytical predictions are relevant.

When the flow is very compressible, it is not possible to apply these analytical techniques and simulations must be used. Kim & Ryu (2005) perform a series of isothermal simulations at various Mach numbers. They find that at low Mach numbers (say $\mathcal{M} \simeq 1$), the density power spectrum is close to the theoretical predictions described in the previous paragraph, *i.e.* is roughly proportional to $k^{-5/3}$. At higher Mach numbers, it gradually becomes shallower with exponents that could become as small as -0.7 . The reason seems to be due to the term $\rho \nabla \cdot \mathbf{v}$ in the continuity equation because the density power spectrum is then related to the power spectrum of this term. Indeed, in the high Mach number case, the strong shocks create thin shocked layers in the flow which resemble Dirac functions. As their power spectra are $\propto k^0$, it is expected to get exponent power spectra close to this value and thus much shallower than the subsonic case.

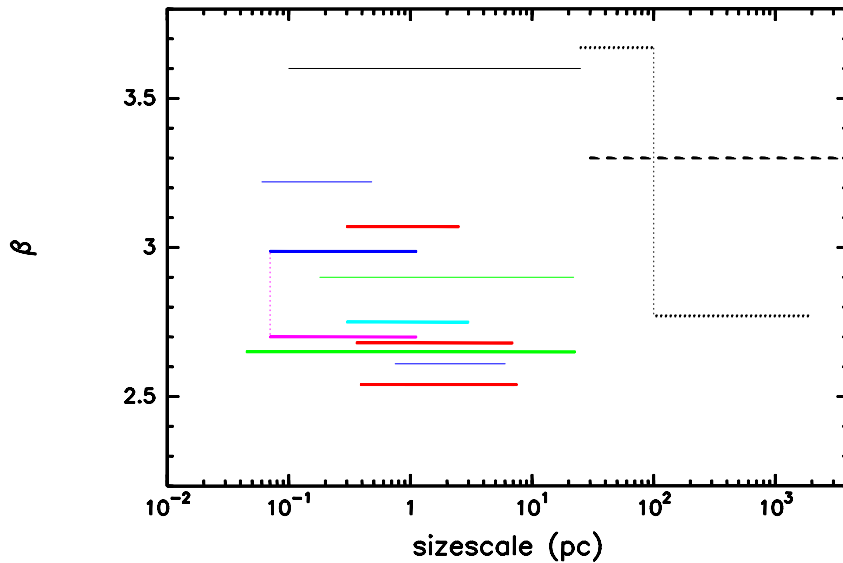


Fig. 10 Spectral indices β of emission maps versus the range of size scales where the power-law $P_I(k) \propto k^{-\beta}$ is observed. Indices for dust emission (green), ^{12}CO (blue and purple) and ^{13}CO (red) line emission, HI emission (black) and absorption (turquoise) are obtained with various methods (see text for details). The error bars (not shown for clarity) on all the values of β vary between 0.01 and 0.3.

On the other hand, when the equation of continuity is formulated using $s = \log \rho$ instead of ρ , it simply becomes $d_t s = -\nabla \cdot \mathbf{v}$ which suggests that the variable s should be less affected by this effect. Indeed various authors have computed the power spectrum of s , both in the isothermal and two-phase cases (Beresnyak et al. 2005, Schmidt et al. 2009, Audit & Hennebelle 2010) and they all find that the exponent of the power spectrum of s is always not too far from the Kolmogorov exponent although no rigorous analytical prediction has been made so far.

4.2.2 Power spectra: observations

Figure 10 displays the power spectral indices β of an ensemble of intensity (I) maps versus the range of size scales over which the power-law $P_I(k) \propto k^{-\beta}$ is observed. Various methods are used. The Δ -variance method, introduced by Stutzki et al. (1998), has been used on maps of line integrated areas (*i.e.* close to column density maps) of CO emission in molecular clouds (Bensch et al. 2001): $^{13}\text{CO}(1-0)$ in star-forming regions (red lines), $^{12}\text{CO}(1-0)$ and $^{13}\text{CO}(1-0)$ in the Polaris Flare (blue thin lines). In the $^{12}\text{CO}(2-1)$ line, two values are shown (connected by a dotted line): for the whole line emission (thick blue) and for the line-wing emission only (purple) (Hily-Blant private communication).

Slopes of dust emission power spectra are shown in green: IRAS $100\mu\text{m}$ emission of the high galactic latitude sky (thin) (Gautier et al. 1992) and *Herschel*/SPIRE $250\mu\text{m}$ emission combined to IRAS $100\mu\text{m}$ in the Polaris Flare (thick) (Miville-Deschênes et al. 2010). The constancy of β over almost three orders of magnitude in scales obtained with the SPIRE data (Figure 10) is impressive. It hides, however,

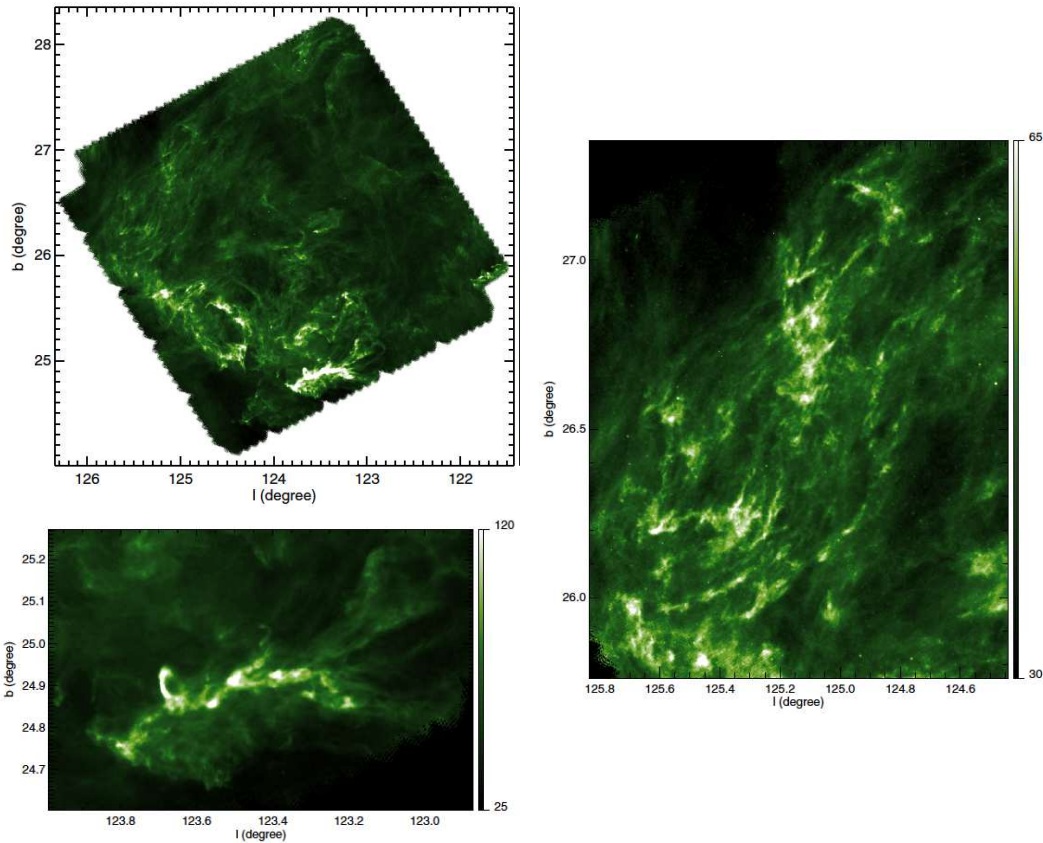


Fig. 11 **Left:** *Herschel*/SPIRE $250\mu\text{m}$ map of the Polaris Flare over $\sim 7\text{pc} \times 7\text{pc}$. Units are MJy sr^{-1} (*top*). Subfield of the region of largest column density discussed in Sect. 3.6 (*bottom*). **Right:** Another subset of regions of lowest column density. Note the brightness difference. (from Miville-Deschênes et al. 2010).

the intrinsic diversity of small scale structures illustrated in the two subsets of Fig. 11.

Slopes of HI emission power spectra are displayed in black: Large Magellanic Cloud (thick dotted) (Elmegreen et al. 2001), Small Magellanic Cloud (thick dashed) (Stanimirovic & Lazarian 2001). Galactic HI in emission: North Polar Spur (thick solid) (Miville-Deschênes et al. 2003a). The slope of the power spectrum of Galactic HI in absorption is in turquoise: VLBI maps of HI absorption optical depth against Cas A (Deshpande et al. 2000). Values derived from HI emission are predominantly WNM values, those from HI in absorption relate to the CNM. In the LMC, a slope discontinuity is observed, and two values of β (connected by a dotted line) are displayed over each relevant range of scales. This change of slope is ascribed to the transition from 2- to 3-dimensional turbulence at about 100 pc, the estimated thickness of the HI layer in the LMC according to the criterion of Lazarian & Pogosyan (2000).

Figure 10 provides quantitative insights on the link between turbulence in the diffuse medium and that in molecular clouds. First, the values of $\beta = 3.6$

obtained from HI in emission are significantly larger than those obtained from HI in absorption $\beta = 2.75$. Second, a value of $\beta = 2.75$ is similar to the values inferred from dust emission at similar scales. Cold dust emission at small scale (≤ 0.5 pc), however, has a significantly flatter spectrum ($\beta = 2.65$) than that of $^{12}\text{CO}(2-1)$ ($\beta = 3$), but is remarkably similar to that of CO line-wing emission ($\beta = 2.7$). This illustrates the fact that at small scales, CO emission of molecular clouds appears almost featureless in maps of integrated intensity, due to projection (not optical depth) effects. Structure is detectable only in the velocity field, supporting a close link between gas dynamics and the formation of structures. Indices even higher than $\beta = 3$ have been obtained in the Perseus complex by Sun et al. (2006) with a small dynamic range of scales.

These results are qualitatively in good agreement with the trends inferred in the previous section. In particular, the HI seen in emission (predominantly WNM), which is not very supersonic on large scales, presents an index β close to $11/3$. The CO and the HI in absorption, which both trace colder supersonic media, have power spectra that are much shallower and reminiscent of what is obtained in numerical simulations for high Mach number flows. The trend of the index being higher at smaller spatial scales may also signal the transition from the supersonic regime to the subsonic one. Indeed, the sonic length is typically of the order of 0.1 pc, a scale around which the value of β seems to increase significantly.

Alternatively, the increase of β toward small scale, found from the values derived from CO maps, may be seen as a manifestation of the multi-fractal facet of CO molecular clouds. As shown by Stutzki et al. (1998), there is a relation $\beta = \gamma(3 - \alpha)$ between the slope β of the power spectrum of a fractal Brownian motion (fBm) structure, the index γ of the mass-size relation $M \propto l^\gamma$, and the slope of the mass spectrum α . Since α does not vary (see previous section) among molecular clouds, the increase of β from 2.2 to 3.2 is nothing more than the steady increase of the fractal dimension of the cold ISM as the size scale decreases, *i.e.* a decrease of lacunarity in the maps. However, it cannot be ruled out that the variation of β is not gradual but abrupt and, alike HI, is a manifestation of the dimensionality of molecular clouds: the increase of β at about 1 pc would suggest that molecular clouds (and CNM clouds) are sheet-like structures of thickness ~ 1 pc.

Incidentally, the spectral index $\beta = 3.6$ of the power spectrum of the HI integrated emission (*i.e.* the HI column density) in the North Polar Spur is the same as that found for the line velocity centroid maps. Miville-Deschênes et al. (2003b) have shown, by using fBm simulations, that in the case of an optically thin medium, the former is the spectral index of the 3-dimensional density field and the latter, that of the velocity field. The value $\beta = 3.6$ being consistent with the Kolmogorov scaling of incompressible turbulence, the galactic HI value in emission (also found in other samples) provides one more example of Kolmogorov scaling found in the compressible interstellar turbulence (see Federrath et al. 2008).

4.2.3 Mass-size relation

Some authors have attempted to characterise the mass-size relation in numerical simulations using various techniques (see e.g. Federrath et al. 2009). The so-called mass size method has been applied by Kritsuk et al. (2007) and Federrath et al. (2009). It consists in considering a series of boxes of size l centered around all

density peaks and counting the mass, $M(l)$ within the box. The recovered $M(l)$ has the form of a power-law, $M(l) \propto l^\gamma$. The exponent γ has been measured to be 2.39 according to Kritsuk et al. (2007) and 2.11 with solenoidal forcing and 2.03 for compressible forcing according to Federrath et al. (2009) who count only the mass above half the value of the local maximum.

Another way to estimate a mass-size relation which is closer to observations, though still significantly different, is to clip the density field choosing a density threshold and to reconstruct the structures using a friend of friend algorithm, i.e. gathering all connected cells. Then, the mass of each identified structure can be easily obtained. The size can be estimated either by taking the most distant cells or by computing and diagonalizing the inertia matrix and taking the largest eigenvalue. Plotting M against l , Audit & Hennebelle (2010) find that the relation is again close to a power-law $M \propto l^{2.3-2.5}$ both for isothermal and two-phase flows.

Considering that gravity is not included in these simulations, the physical origin of the mass-size relation can only be attributed to turbulence. Yet, no quantitative explanation has been inferred neither for the power-law behaviour nor the measured exponent. A phenomenological model has been proposed by von Weizsäcker (1951) and Fleck (1996) who postulate a hierarchy of density fluctuations at successive scales given by

$$\frac{\rho_\nu}{\rho_{\nu-1}} = \left(\frac{l_\nu}{l_{\nu-1}} \right)^{-3\alpha}. \quad (4)$$

This leads to a mass-size relation $M \propto l^{3-3\alpha}$ which suggests that $\alpha \simeq 0.1-0.2$. The interesting point is that, assuming the phenomenology of Kolmogorov still holds in the compressible case (*i.e.* $\rho v^3 \propto l$), one gets $v \propto (l/\rho)^{1/3}$, which leads to $v \propto l^{1/3+\alpha}$ and the power spectrum of v , $P_v(k)$ is thus proportional to $k^{-5/3-2\alpha}$ (since $\langle v^2 \rangle \propto \int_{k_v}^{\infty} P_v(k) k^2 dk$). This offers a valuable explanation for a velocity field power spectrum being steeper in the compressible case than in the incompressible case, since the exponent is on the order of -2. Using this expression, Kritsuk et al. (2007) measure the exponent to be $\alpha \simeq 0.15$.

As shown in Fig. 5, the mass size relation inferred from observations is also a power-law with an exponent $\gamma \simeq 2-2.3$ and therefore close to what is measured in numerical simulations. Although this apparent agreement is interesting, we recall that the CO clumps are determined using both spatial and kinematic information, *i.e.* in the position-position-velocity (PPV) space while the structures described above are defined using the 3D density field, independently of the velocity. Whether the two approaches select the same structures is not clear at this stage. Using periodic boxes, Ostriker et al. (2001) show that the structures selected in the PPV-space are sometimes not spatially continuous. On the other hand, in the context of colliding flows, Heitsch et al. (2009) use the PPV methods to identify the structures and find a good correspondence with the structures identified using 3D spatial information. This issue certainly requires further careful investigation.

4.3 Mass spectra of clumps and cores

4.3.1 Some observational results

To date, the mass spectra of two types of cloud have been convincingly inferred from observations, namely the so-called CO clumps and the prestellar cores. As recalled in section 3.5, the mass spectrum of the CO clumps identified in the PPV-space obeys the same power-law $dN/dM \propto M^{-1.8}$, over about 7-8 orders of magnitude in mass.

The core mass spectrum (CMF) has been first obtained by Motte et al. (1998), Testi & Sargent (1998), Johnstone et al. (2000) and more recently by Alvés et al. (2007) and André et al. (2010). The derivations did not make use of the velocity information but are based only on the spatial distribution. It has been pointed out that at masses larger than $\simeq 1M_{\odot}$ the dense core distribution is compatible with a power-law significantly steeper than that of the CO clump power spectrum with an exponent close to the value 2.3 inferred by Salpeter (1955) for the initial mass function, $dN/dM \propto M^{-2.3}$ (or equivalently $dN/d\log M \propto M^{-1.3}$). At lower core mass, the most recent studies claim to see a change in the distribution with a pronounced flattening and possibly a peak around $0.5 - 1M_{\odot}$ (André et al. 2010). In general, it is found that the CMF is very similar in shape to the IMF, but shifted towards larger masses by a factor of about 3.

It is not easy to find a theory which accounts for all these facts simultaneously. In particular, we would like to account for the fact that *i*) the relation $dN/dM \propto M^{-\alpha}$ with $\alpha \simeq 1.8$ extends over 7-8 orders of magnitude and applies both to CO clumps which are self-gravitating (e.g. $M > 10^3 M_{\odot}$) and CO clumps which are not; *ii*) while the dense cores are self-gravitating entities, their mass distribution is different from the most massive clumps which are also self-gravitating. Different approaches recently developed lead to a possible explanation. A strong hint in this direction comes from the work of Peretto & Fuller (2010) who have shown that while the mass distribution within the infrared dark clouds (IRDC) resembles the mass spectrum of the CO clumps, the mass distribution of their fragments, *i.e.* the density fluctuations within the IRDC resembles the mass spectrum of the dense cores. This clearly calls for a unifying interpretation.

4.3.2 Mass spectra of turbulent non self-gravitating clouds

Let us start with elementary considerations which suggest that indeed $dN/dM \propto M^{-2}$ is a natural power spectrum in a 3D space. In the Fourier space, the volume occupied by fluctuations of wavenumber between k and $k + dk$ is $4\pi k^2 dk$. It seems reasonable to assume that for a broad variety of situations, $dN(k) \propto k^2 dk$. Now, in 3D we expect that the mass of a clump can be simply proportional to its volume, that is $M \propto R^3$. Therefore $dM \propto k^{-4} dk$ and thus $dN/dM \propto k^6 \propto M^{-2}$. It is interesting to stress that the power spectrum of the CO clumps and the high-mass part of the dense core distributions have exponents close to -2. The exponent -2 is also the value for which the mass is equally distributed between cores of low and high mass since $\int_{M_{min}}^{M_{max}} dN/dM dM \propto \ln(M_{max}/M_{min})$. Beyond these elementary considerations, it is clearly necessary to infer the mass spectrum of the different types of cloud from the specific physical processes that drive their evolution.

As CO clumps are presumably density fluctuations, it seems natural to relate their mass spectrum to the statistical properties of the density field, likely a consequence of supersonic turbulence. The first attempt along this line has been made by Stutzki et al. (1998) who relate the column density power spectrum index, β , the mass-size relation index, γ and the clump mass spectrum index, α through the relation: $\beta = (3 - \alpha)\gamma$. This follows from calculating the column density power spectrum as a sum of Gaussian clumps. It suggests that the mass-size relation and the distribution of clumps are related (see also Elmegreen & Falgarone 1996). More recently, Hennebelle & Chabrier (2008) have performed a multi-scale analysis following the approach developed in cosmology by Press & Schechter (1974). They assume that the density PDF is log-normal and that the power spectrum exponent of $s = \log \rho$ is close to the Kolmogorov exponent, $P_s(k) \propto k^{-n'}$ with $n' \simeq 11/3$. In this way, they obtain the relation $\alpha = 3 - n'/3$ or equivalently $n' = (3 - \alpha) \times 3$, a relation quite similar to that obtained by Stutzki et al. (1998) with some important differences. First, while β is the power spectrum index of the *column density field* (or equivalently the density field), n' is the power spectrum index of $\log(\rho)$. Second, while the coefficient γ must be specified in the approach of Stutzki et al. (1998), Hennebelle & Chabrier (2008) do not introduce this parameter which can be deduced from the calculations as emphasized in Chabrier & Hennebelle (2010). Note that the power spectrum indices of ρ and $\log(\rho)$ are different especially at high Mach numbers where density contrasts are high and the gas is organised in clumps that do not fill the volume. Indeed, these two expressions for α can be combined leading to $n' = 3\beta/\gamma$. This in turn suggests that for highly supersonic flows, the smaller values of β result in a more lacunary medium.

The mass spectra of non self-gravitating clumps, *i.e.* clumps induced by pure turbulence, have been obtained numerically by Hennebelle & Audit (2007), Heitsch et al. (2008), Dib et al. (2008), Audit & Hennebelle (2010) and Inoue & Inutsuka (2012). These authors have simulated various types of flow including isothermal and two-phase medium as well as periodic boxes and colliding flows. In each case the mass spectrum has been inferred to be compatible with a power-law with $\alpha = 1.7-1.8$ similar to the mass spectrum of the CO clumps and to the analytical prediction, $\alpha = 3 - n'/3$, mentioned above. Considering that both the input physics and the boundary conditions are different in these studies, the lack of variations for the measured α strongly suggests that it is the very nature of turbulence that determines almost entirely the value of α while cooling, instabilities and forcing play a secondary role.

4.3.3 Mass spectra of self-gravitating clouds

The mass spectrum of self-gravitating condensations has been inferred by Padoan et al. (1997) assuming a log-normal density distribution and considering thermal support only. Hennebelle & Chabrier (2008, see also Hennebelle 2012) include the turbulent support that resists gravity and show that it is crucial to predict the mass spectrum. They use the same formalism than for the turbulent fluctuation case described previously, but instead of adopting a simple uniform density criterion, require that the parcel of gas should be dominated by its own gravity. More precisely they perform a multi-scale analysis and select the mass enclosed in the smallest scale at which a given piece of gas is self-gravitating. The distribution they infer is very similar in shape to the core mass function (e.g. André et al. 2010) and

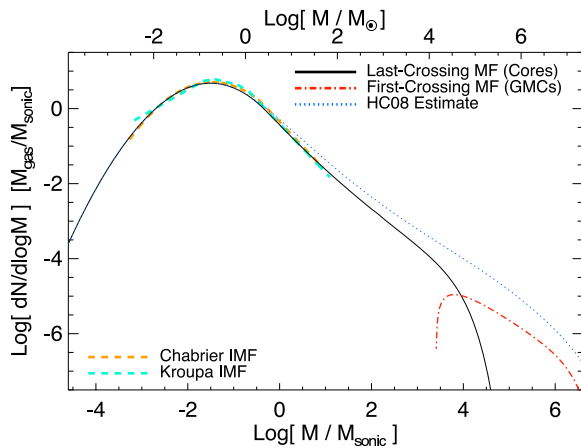


Fig. 12 Core mass spectrum and GMC mass spectrum as calculated by Hopkins (2012b). The blue dotted curve shows the core mass function inferred by Hennebelle & Chabrier (2008) while the solid and dot-dashed lines show structures defined by the last and first crossing of the self-gravitating barrier.

to the initial mass function (e.g. Kroupa 2002, Chabrier 2003). In particular the slope at high masses is similar to the Salpeter (1955) estimate $dN/d\log M \propto M^{-x}$, $x \simeq 1.35$. At low masses the distribution presents a peak and its overall shape is close to a log-normal distribution.

Recently, Hopkins (2012a,b) improves on this approach by applying the excursion set theory (Bond et al. 1991) which consists in making a random walk in the Fourier space of the density field and counting the density fluctuations that cross the requested barrier, *i.e.* reach a requested density threshold. Hopkins presents a global model that includes the spatial scales larger than the molecular clouds appropriate for a description of the whole galactic disc. An interesting result is that the clouds defined as entities which cross first the requested self-gravitating barrier have a mass spectrum which is slightly shallower than M^{-2} while the condensations defined by the last crossing of the barrier have a mass spectrum almost identical to that by Hennebelle & Chabrier (2008) except at large masses. This is illustrated in Fig. 12. An obvious interpretation is that the first type of structures likely represents the massive molecular clouds that are not themselves embedded into a larger self-gravitating cloud while the second type can possibly be associated to the prestellar core progenitor. Indeed it suggests that, while large scale self-gravitating clumps should have a mass spectrum close to $M^{-1.8-2}$, the mass spectrum of the smallest self-gravitating fluctuations, likely to be the core progenitors, should be close to the core mass function.

Interestingly, the mass spectrum for the purely turbulent clumps as inferred by Hennebelle & Chabrier (2008, see sect. 4.3.2) and that of the largest self-gravitating clumps obtained by Hopkins (2012b) are both power-laws with very similar exponents. This is an appealing explanation for the mass spectrum of the CO clumps apparently constant over almost 9 orders of magnitude in mass (e.g. Heithausen et al. 1998, Kramer et al. 1998) even though the most massive ones are self-gravitating while the least massive are not, with the transition occurring at $10^2 - 10^3 M_{\odot}$. A possible route for the least massive self-gravitating ones is that

they originated by turbulent decay within non self-gravitating clumps and that gravity eventually took over during the condensation process through cooling and energy dissipation. In this case, the part of the CO clump mass spectrum which is due to turbulence could be extended towards higher masses. On the other hand, the formation of the most massive clumps may have been initially triggered by their own self-gravity. It is probably difficult at this stage to estimate where the possible transition between the two regimes appears.

It must be noted that CMF in good agreement with the observed distributions have also been constructed using different approach and assumptions. For example Myers (2009a) suggests a model based on gas accretion in dense cores with a distribution of infall durations. Kunz & Mouschovias (2009) develop a model based on magnetically dominated cores assuming a log-normal distribution of magnetic fluxes.

Finally, the CMF has also been inferred from various numerical simulations. Using hydrodynamical and MHD simulations without gravity, Padoan et al. (2007) identify the cores as the density fluctuations induced by turbulence that would have been self-gravitating. Considering pure thermal support (as in Padoan et al. 1997), they find that the CMF produced is too steep. When thermal plus magnetic support is taken into account, the core mass function is found to have a Salpeter-like slope. Schmidt et al. (2010) perform similar hydrodynamical simulations and analysis but include the turbulent support in the core definition. They find that the CMF is a power-law at high masses whose index is close to the Salpeter exponent while it is too steep when only thermal support is included in the core definition. Performing quantitative comparisons with the predictions of Hennebelle & Chabrier (2008), they infer a good agreement. Smith et al. (2009) carry out simulations that include both turbulence and self-gravity and define the cores using the potential wells. They also find a CMF close to that observed. All these results underscore the importance of non-thermal support to reproduce the observed CMF.

4.4 Filaments

With the increased sensitivity of CO observations and the availability of larger maps away from the brightest spots coinciding with star forming regions, the evidence for the filamentary structure of the CO emission became clear (e.g. Ungerechts & Thaddeus 1987, Bally et al. 1987). At about the same time, the far-IR all-sky IRAS survey (Low et al. 1984) revealed the ubiquitous filamentary structure of the ISM, and discovered the cirrus clouds, *i.e.* the filamentary structure of the diffuse ISM. This suggested a link between filaments in the diffuse medium and more opaque filaments. Abergel et al. (1994) showed quite convincingly that the filaments of cold dust were those of largest column density ($N_{\text{H}_2} \geq 10^{22} \text{ cm}^{-2}$) seen in ^{13}CO only and invisible in the ^{12}CO maps because of the high opacity of $^{12}\text{CO}(1-0)$ in diffuse molecular gas.

Subsequently, several mid-infrared surveys of the inner Galaxy (*ISO*, Pérault et al. 1996, *MSX*, Price et al. 2001, *Spitzer/MIPS*, Benjamin et al. 2003) revealed the existence of massive filamentary structures of cold dust, seen as dark lanes against the bright galactic background emission. These regions are now known as infrared dark clouds (IRDC). One of the most spectacular IRDC is the Nessie nebula with

a linear extent of 80 pc long and a width of only 0.5 pc thick. The linear mass density is still poorly constrained (Jackson et al. 2010).

4.4.1 Self-gravitating filaments

The presence of filaments in molecular clouds and their active role in the star formation process has long been recognized and is particularly suggested by the presence of dense cores often elongated in the same direction (Tachihara et al. 2000) and sometimes periodically distributed (e.g. Dutrey et al. 1991). Moreover, in the case of the Taurus molecular cloud, Hartmann (2002) shows that the protostars distribution closely follows the filament network identified by Mizuno et al. (1995). The association of filaments and cores suggests that the latter likely form from the gravitational fragmentation of the filaments, a process supported by analytical studies (e.g. Stodolkiewicz 1963, Ostriker 1964, Larson 1985, Inutsuka & Miyama 1992, Fiege & Pudritz 2000a, Curry 2000), which in particular show that in the isothermal case there is a critical line mass (mass per unit length) equal to $2c_S^2/G$ for which equilibrium is possible leading to a density profile

$$\rho(r) = \frac{\rho_0}{(1 + r^2/l_0^2)^2}, \quad l_0 = \left(\frac{2c_S^2}{\pi G \rho_0} \right)^{1/2}. \quad (5)$$

where c_S is the sound speed. This equilibrium solution is, however, subject to gravitational instabilities. The growing fluctuations would give birth to cores separated by a few Jeans lengths, which corresponds to the typical wavelength of the fastest unstable mode.

The formation mechanism of these self-gravitating filaments is still not well understood yet but a few theoretical arguments are worth considering. The most important point is that gravity tends to amplify any pre-existing anisotropy, as emphasized for example by Lin et al. (1965). This is simply because the force is the gradient of the gravitational potential and is thus higher along the shortest direction. This implies that a gravitational structure which would be slightly elongated, for example because of the way it was assembled, will quickly become very elongated. Another way for filament formation is by gravitational instabilities of self-gravitating layers, as shown for example by Spitzer (1978) and Nagai et al. (1998). The expression of the density profile of the layers is given by

$$\rho(z) = \frac{\rho_0}{\text{ch}(z/l_0)^2}, \quad l_0 = \left(\frac{c_S^2}{2\pi G \rho_0} \right)^{1/2}. \quad (6)$$

Again, filaments will be periodically distributed with separation of a few Jeans lengths. Interestingly, Nagai et al. (1998), who performed linear stability analysis of a magnetized self-gravitating layer, show that the orientation of the most unstable mode tends to be correlated with the magnetic field direction. The result depends on the external pressure that determines the scale height, z_b at which the solution is truncated. If $z_b \gg l_0$ then the fastest growing mode is aligned with the magnetic field, resulting in filaments which are perpendicular to the field direction. The physical reason is that, since the width is large relative to the Jeans length, the layer is compressible and density fluctuations are easier to develop along the magnetic field. On the other hand when $z_b \ll l_0$, the fastest growing

mode is perpendicular to the magnetic field and the filaments are aligned with it. This is because the layer is almost incompressible (since the scale height is smaller than the Jeans length), thus the instability develops through the bending of the layer. As perturbations whose wave vectors are perpendicular to the magnetic field do not bend the field lines, these perturbations develop more easily. A nice bidimensional solution which describes the continuous and quasi-static evolution from the self-gravitating layer to the self-gravitating filament has been derived by Schmid-Burgk (1967). It is given by

$$\rho(x, z) = \frac{\rho_0(1 - A^2)}{(\operatorname{ch}(z/l_0) - A \cos(x/l_0))^2}. \quad (7)$$

When $A = 0$, it is simply reduced to the self-gravitating layer while when $A \rightarrow 1$, it tends to a set of discrete periodic filaments. Recently, this solution has been used by Myers (2009b) to model the hub filament structures that are often observed around young stellar groups. In this model, a self-gravitating layer forms first, then it fragments in filaments as predicted theoretically. Owing to the presence of local overdensities, the filaments converge towards each other forming a denser and more massive region, which eventually give birth to a star cluster.

4.4.2 A continuum of filaments

Thanks to its unprecedented sensitivity and large-scale mapping capabilities, Herschel/SPIRE has now provided a unique view of these filamentary structures of cold dust (e.g. Miville-Deschênes et al. 2010, Ward-Thompson et al. 2010, André et al. 2010). One of the main findings of the SPIRE observations is the very large range of column densities – a factor of 100 between the most tenuous ($N_{\text{H}_2} = 2 \times 10^{20} \text{ cm}^{-2}$) and most opaque ($N_{\text{H}_2} \sim 10^{23} \text{ cm}^{-2}$) of the observed filaments in several fields (Fig. 8) contrasting with a narrow range of filament width (between 0.03 and 0.2 pc) barely increasing with the central column density (Arzoumanian et al. 2011).

Understanding this unexpected result is challenging. First, one would naively expect that self-gravitating filaments would have a thickness comparable to the Jeans length at odds with the observations (see figure 7 of Arzoumanian et al. 2011). Second the very existence of such thin structures in a turbulent medium is not at all straightforward. One possibility is that it corresponds to the sonic length. Indeed, if filaments are produced in shocks, then their density, ρ_f , should be linked to the background density, ρ_0 by the Rankine-Hugoniot relation: $\rho_f = \rho_0 \mathcal{M}^2$, where \mathcal{M} is the Mach number, $\mathcal{M} = v/c_S$. The velocity on the other hand is linked to the scale as $v(L) \simeq v_0(L/1\text{pc})^\eta$ which is simply the Larson relation discussed above and $v_0 \simeq 0.8 \text{ km s}^{-1}$ while $\eta \simeq 0.4 - 0.5$. As the size of the shocked layer is simply given by $L_f = L\rho_0/\rho_f$, we get $L_f = (c_S/v_0)^2 \times L(L/1\text{pc})^{-2\eta}$. In particular assuming that $\eta = 0.5$, the shocked layer becomes independent of the fluctuation size and with $c_S \simeq 0.2 \text{ km s}^{-1}$, we get $L_f \simeq 0.07 \text{ pc}$ which is close to the thickness inferred by Arzoumanian et al. (2011). However, there are a couple of intriguing issues with this explanation. First, the derived scale is the typical thickness of the shocked layers and not of the filaments, thus one step is missing to go from the layer to the filament. Second, it has assumed that the gas is isothermal. Thus once the velocity fluctuation has vanished (typically in a few

crossing times L/v), the filament re-expands due to the over-pressure relative to the ambient medium. In a few sound crossing times L_f/c_S , the thickness broadens significantly therefore leading presumably to a wide thickness distribution. This scenario is somehow similar to that proposed by Padoan et al. (2001) which show that, in their simulations, the filaments correspond to low velocity regions and are often found at the intersection between shocked layers.

Recently, an alternative explanation has been proposed by Fischera & Martin (2012) who argue that the characteristic size of the filaments is simply the result of mechanical equilibrium in the radial direction. Assuming that the filaments are pressure bounded, they find that the equilibrium of the isothermal gas, between thermal pressure and gravity leads to a diameter of about 0.1 pc with a weak dependence on the column density. We must stress that no detailed analysis, however, on the exact nature of filaments ubiquitously found in numerical simulations has been performed to date. There is, however, a general visual trend of MHD simulations that appear more filamentary than hydrodynamical simulations (e.g. Padoan et al. 2007, Hennebelle et al. 2008). If confirmed by quantitative arguments, this trend could suggest that shocks are only part of the process. Indeed, it is likely the case that the shear which is at the very heart of turbulence should also play a role in filament formation.

In this regard, the dynamic origin of filaments is observationally supported by the remarkable coincidence between one of the faintest filaments detected by SPIRE in the Polaris Flare (Fig 11, bottom left), also visible as a weak CO filament, and the parsec-scale coherent structure of intense velocity-shear discussed in section 3.7.1 (Hily-Blant & Falgarone 2009). Whether the velocity-shear is associated with a true compression due to a shock propagating in the plane of the sky cannot be decided because of projection effects.

4.4.3 The most tenuous filaments

Tenuous filaments are interesting structures since they may shed light on the origin of filaments and a possible growth scenario, but they are difficult to study for obvious reasons. A tenuous filament connected to a low-mass dense core of the Taurus cloud has been thoroughly studied in different ^{12}CO transitions and isotopes (Falgarone et al. 2001). It is a spinning filament, with a density drop-off as steep as $n_{\text{H}_2}(r) \propto r^{-4}$. Periodic oscillations of its azimuthal velocity have been found. Its average inner pressure, including a turbulent contribution, exceeds by a factor ~ 10 the surface pressure, even including the contribution due to the self-gravity of the Taurus complex. It has a low mass-to-virial mass ratio m/m_{vir} (here, the mass is the linear mass), hence it is not held together by self-gravity. It is possibly confined by helical magnetic fields because the periods of the observed wavelike behaviors of the velocity field are reminiscent of the instability signatures computed by Fiege & Pudritz (2000ab) for filaments threaded by such fields. In this framework, the fragment separation observed along this tenuous filament suggests a toroidal magnetic flux five times larger than poloidal.

5 Magnetic fields in molecular clouds

5.1 Theoretical considerations

Early on, magnetic fields have been proposed to provide an important mechanical support to the gas (see e.g. Shu et al. 1987), possibly explaining the low star-formation efficiency within the Milky Way. This suggestion has contributed to trigger studies of interstellar magnetic fields. Although, as described below, the actual trend indicated by measurements of the magnetic intensity is that magnetic fields, although dynamically important, may be not dominant, we recall below the theoretical elements that were put forward in support of the magnetically regulated star formation theory.

5.1.1 Magnetic support

Magnetic forces are highly non-isotropic. An easy way to estimate the strength of magnetic support is to compute the ratio of the magnetic over gravitational energies. For simplicity, let us consider a spherical and uniform cloud of mass M , volume V , radius R , threaded by a uniform magnetic field, of strength B . The magnetic flux within the cloud, Φ is equal to $\Phi = \pi R^2 B$. As long as the magnetic field remains well coupled to the gas, the magnetic flux threading the cloud will remain constant with time. The ratio of magnetic over gravitational energies for uniform density cloud threaded by a uniform magnetic field, is

$$\frac{E_{\text{mag}}}{E_{\text{grav}}} = \frac{B^2 V}{8\pi} \times \frac{2R}{5GM^2} \propto \frac{B^2 R^4}{M^2} \propto \left(\frac{\Phi}{M}\right)^2. \quad (8)$$

Remarkably, the ratio of magnetic over gravitational energies is independent of the cloud radius. This implies that if the cloud contracts or expands, the relative importance of these two energies remains the same. This is unlike the thermal energy of an isothermal gas, which becomes smaller and smaller compared to the gravitational energy as the cloud collapses. It is clear from Eq. 8, that there is a critical value of the magnetic intensity for which the gravitational collapse is impeded even if the cloud was strongly compressed. Mouschovias & Spitzer (1976) have calculated accurately the critical value of the mass-to-flux ratio using the virial theorem and numerical calculations of the cloud bidimensional equilibrium. A cloud which has a mass-to-flux ratio smaller than this critical value cannot collapse and is called subcritical. It is called supercritical when the mass-to-flux is larger than the critical value. It is usual to define $\mu = (M/\Phi)/(M/\Phi)_{\text{crit}}$. Large values of μ correspond to small magnetic fields and thus supercritical clouds.

5.1.2 Ambipolar diffusion

One of the problems with magnetic support is that when ideal MHD applies, the field remains strong and prevents collapse. Mestel & Spitzer (1956) have first considered the possibility of leakage of the magnetic flux which would reduce the strength of the field. At microscopic scales, the neutrals are not experiencing the Lorentz force which applies only on charged particles. Strictly speaking, this implies that at least two fluids should be considered, the neutrals and the ions (in

different contexts more than one fluid of charged particles must be considered), to treat the problem properly. Since the two fluids are coupled to each other by collisions, the neutrals are nevertheless influenced by the magnetic field if the gas is sufficiently ionized. Since the ionization in molecular clouds is usually of the order of 10^{-7} , the density of the ions is much smaller than the density of the neutrals. It is thus possible to neglect the inertia of the ions. A strong assumption however is that of the equilibrium between the Lorentz force and the drag force exerted on the ions. This leads to

$$\frac{(\nabla \times \mathbf{B}) \times \mathbf{B}}{4\pi} = \gamma \rho \rho_i (\mathbf{v}_i - \mathbf{v}), \quad (9)$$

where ρ_i and v_i are the ion density and velocity respectively, $\gamma \simeq 3.5 \times 10^{13} \text{ cm}^3 \text{ g}^{-1} \text{ s}^{-1}$ is the drag coefficient (Mouschovias & Paleologou 1981). From Eq. 9, the ion velocity can easily be expressed as a function of the neutral velocity and the Lorentz force. Considering now the induction equation, which involves the velocity of the ions, and using Eq. 9, we obtain

$$\partial_t \mathbf{B} + \nabla \times (\mathbf{B} \times \mathbf{v}) = \nabla \times \left(\frac{1}{4\pi\gamma\rho\rho_i} ((\nabla \times \mathbf{B}) \times \mathbf{B}) \times \mathbf{B} \right). \quad (10)$$

The left part of this equation is identical to the induction equation except that the velocity of the neutrals appears instead of the velocity of the ions. The right term is directly responsible for the slip between the neutrals and the magnetic field. Although it is of the second order, it is not rigorously speaking a diffusion term. From this equation, there can be easily inferred a typical time-scale for ambipolar diffusion

$$\tau_{\text{ad}} \simeq \frac{4\pi\gamma\rho\rho_i L^2}{B^2}, \quad (11)$$

where L is the typical spatial scale relevant for the problem. In the context of star-formation, L could be the size of the cores, R . Ionization equilibrium allows to estimate that the ions density is about $\rho_i = C\sqrt{\rho}$, where $C = 3 \times 10^{-16} \text{ cm}^{-3/2} \text{ g}^{1/2}$.

If a dense core is initially subcritical (therefore magnetically supported), the diffusion of the field will progressively reduce the magnetic flux within the cloud. So after a few ambipolar diffusion times, the cloud becomes supercritical and the magnetic field cannot prevent the collapse any more. The important and interesting question at this stage is ‘‘How much is the collapse delayed by this process?’’ In order to estimate this time, it is usually assumed that the cloud is in virial equilibrium, $B^2/4\pi \simeq M\rho G/R$ (within a factor of a few) and to compute the ratio of τ_{ad} and τ_{ff} , the free-fall time (Shu et al. 1987). This leads to:

$$\frac{\tau_{\text{ad}}}{\tau_{\text{ff}}} \simeq 8. \quad (12)$$

The implication is that ambipolar diffusion can reduce the star-formation rate significantly making it closer to the observed value (e.g. Shu et al. 1987). Numerical simulations of magnetized collapse controlled by ambipolar diffusion have been performed (e.g. Basu & Mouschovias 1995). These simulations are generally one dimensional and assume a thin disk geometry. When the dense core is very subcritical, with values of μ as low as 0.1, Basu & Mouschovias (1995) found that the collapse is significantly delayed and occurs in about 15 free-fall times. For nearly critical cores, $\mu \simeq 1$, the collapse occurs after about $\simeq 3$ free-fall times.

5.1.3 Turbulence in magnetized clouds with ambipolar diffusion

In Sect. 3.2 we have described the properties of MHD turbulence. Here we focus on the studies which have investigated simultaneously the effect of turbulence and ambipolar diffusion in molecular clouds.

Basu & Ciolek (2004) and Li & Nakamura (2005) have presented 2D simulations combining magnetic support (magnetic field lines are parallel to the cloud) and turbulent motions. Since the clouds are initially subcritical, ambipolar diffusion plays an important role as it allows to reduce locally the magnetic flux. Interestingly, it has been found (Li & Nakamura 2005, Li et al. 2008) that in this context, turbulence tends to accelerate the star-formation. This is because turbulence creates stiff gradients, due to the formation of shocks, in which the ambipolar diffusion takes place quickly. Indeed, Eq. 11 shows that the ambipolar diffusion time decreases with the spatial scale, L . A very interesting result is that these simulations are able to reproduce the low star-formation efficiency observed in the Milky Way provided the initial value of μ is small enough (typically $\mu \simeq 1$) and turbulence is sufficiently strong (typically $v_{\text{rms}} \simeq 10 \times c_S$). More recently, these results have been extended to the 3D and multi-phase case by Vázquez-Semadeni et al. (2011).

In 3D simulations including turbulence, gravity and supercritical magnetic fields, it is found that the star-formation rate is reduced by a factor of a few, i.e. the star-formation rate is smaller in a cloud that has a supercritical magnetic field than in the otherwise identical non magnetized cloud (Price & Bate 2008, Padoan & Nordlund 2011), although the exact physical mechanism by which this happens is not well understood.

Last, a series of recent 3D simulations of supersonic turbulence with ambipolar diffusion (Downes & o'Sullivan 2009, Li et al. 2008, 2012, Tilley & Balsara 2010) have emphasized the impact that ambipolar diffusion has on the turbulence properties. They conclude that, as expected, ambipolar diffusion enhances the rate of turbulent dissipation. Also, the power spectra of density, velocity and magnetic fields tend to be steeper. Finally, the synthetic spectra of the neutral and ionic species show that the latter tend to be narrower than the former. The larger velocity dispersion of the neutrals is certainly a consequence of their partial decoupling from the magnetic field. In principle, these effects could be observed.

5.1.4 Magnetic intensity versus density relation

The relation between the magnetic intensity and the gas density is another important input to understand star-formation, as it bears the signature of the gas motions relative to the field lines.

Before describing the results inferred from numerical simulations, it is worth to recall the different behaviors that can be expected. If the contraction occurs along the field lines, then the magnetic field is not amplified and $B \propto \rho^\kappa$ with $\kappa = 0$. If the motion is perpendicular to the field lines, then it is easy to show that ρ/B stays constant (combining the continuity and induction equations) and thus $\kappa = 1$. Note that in this configuration the magnetic pressure is proportional to ρ^2 and therefore quickly halts any contraction. If the contraction is spherical, then the mass enclosed is simply $\propto \rho R^3$ while the magnetic flux is $\propto BR^2$ thus leading to $B \propto \rho^{2/3}$. It is, however, unlikely that a contracting cloud remains spherical, especially if the

magnetic field is not negligible. In this case, it is expected that an equilibrium along the field lines settles leading to $c_S^2 \simeq \phi$, where ϕ is the gravitational potential. The Poisson equation leads $\phi \propto \rho h^2$ where h is the thickness of the cloud along the field lines. Then, as the mass enclosed is now $\propto \rho R^2 h$ while the magnetic flux is still $\propto BR^2$, we get $B \propto c_S \rho^{1/2}$. Basu (2000) has compared the data provided by Crutcher (1999) with this expression and has obtained a good agreement, which improves if the velocity dispersion σ instead of c_S is used. Another even simpler interpretation of this relation is energy equipartition between magnetic and kinetic energy, $B^2/(4\pi) \propto \rho\sigma^2$.

Various simulations of 3D ideal MHD turbulence tend to show that without gravity (e.g. Padoan & Nordlund 1999, Hennebelle et al. 2008, Banerjee et al. 2009), the magnetic intensity weakly depends on the density field. A weak correlation is found with typically $\kappa \simeq 0.1 - 0.2$. This has been interpreted in the context of two-phase flows by Hennebelle & Pérault (2000) as a consequence of the magnetic tension, which tends to unbend the magnetic field lines and to align the magnetic and the velocity fields. This eventually facilitates the gas contraction. In the context of polytropic flows, the weakness of the correlation has been interpreted by Passot & Vazquez-Semadeni (2003) (see also Burkhart et al. 2009) in terms of the fact that the various types of (nonlinear, or simple) MHD wave are characterized by different scalings of the field strength with the density. Indeed while for fast waves, magnetic intensity and density are correlated, they are anti-correlated for slow waves and not correlated for Alfvén waves. Thus, in a turbulent flow in which all kinds of wave pass through a given point, the field strength is a function of the history of wave passages, rather than of the local density. Moreover, the simulations which treat both self-gravity and turbulence find that at high density the magnetic intensity is $\propto \rho^{0.5}$ (e.g. Hennebelle et al. 2008, Banerjee et al. 2009), which accords well with the analytical predictions deduced above.

5.2 Magnetic field measurements and interpretation

Dust polarization measurements in molecular clouds are making impressive progress in the visible and near-IR ranges (polarization of starlight) and in the submillimeter domain (polarization of dust thermal emission). In the former case, large sensitive cameras allow the detection of thousands polarization vectors simultaneously. An example is given in Fig 13 (left) that displays the measurements of Heiles (2000) throughout the field of the Taurus molecular complex and recent measurements by Chapman et al. (2011) that reveal the small scale coherence of the polarization vectors. In the latter case, sensitive bolometer arrays provide maps of polarized emission of dust in dense cores and filaments. The *Planck* all-sky survey will offer a global view of the dust polarized emission in the Galaxy.

These measurements do not provide the magnetic field intensity, but probe a clear decrease of the polarization degree in the interior of dense cores and in the inner parts of the dense filaments (Matthews et al. 2009). There are several possible interpretations of the depolarization, among which: (i) the decrease of the alignment capability of dust grains if spinning sustained by radiative torques drops due to extinction (Lazarian & Hoang 2007), (ii) a helical magnetic field threading cores and filaments (Fiege & Pudritz 2000b).

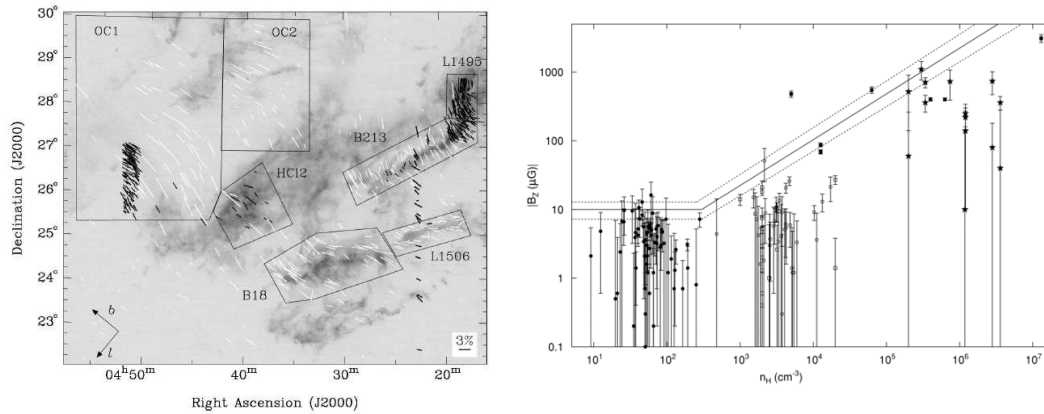


Fig. 13 (*Left*) Polarization vectors of starlight (therefore parallel to magnetic field projection) overlaid on a map of $^{13}\text{CO}(1-0)$ integrated emission of the Taurus complex (Chapman et al. 2011). White lines : Heiles 2000; black lines : Chapman et al. (*Right*) Magnetic field intensity inferred from Zeeman measurements in the HI, OH and CN lines as a function of gas total column density (from Crutcher et al. 2010). The solid line shows the critical mass-to-flux ratio.

The well-known method described by Chandrasekhar & Fermi (1953) to infer the magnetic field intensity from the fluctuations of the polarization angle turns out to be less straightforward than foreseen, although it has been tested in numerical simulations of MHD turbulence (Ostriker et al. 2001). The polarization due to the fluctuations of the larger scale fields in the galactic ISM is contributing to that observed and the separation between the two contributions relies on modelization (see Houde et al. 2009, Hildebrandt et al. 2009). Li et al. (2006) find a correlation of the magnetic field direction in molecular clouds with that in the Galactic plane.

The only direct measurements of the magnetic field intensity are based on the Zeeman effect. Unfortunately, the line frequency shift between left and right circularly polarized emissions is sensitive only to the projection of the magnetic field along the line-of-sight, an effect which is plagued by the signal integration along the line-of-sight itself. Furthermore, given the low magnetic field intensities, there are only a handful of species with large enough sensitivity to the magnetic field to attempt its detection in molecular clouds. These are species with non-zero magnetic moment due to unpaired electrons, for instance (the elusive O_2 , 10^3 less abundant than model predictions, being one of them). So far, the best diagnostics have been OH in diffuse molecular clouds and CN in star-forming regions. All the available results are gathered in Crutcher et al. (2010) and displayed in Fig. 13 (right). They include Zeeman measurements that sample B_{\parallel} in diffuse (mostly atomic) clouds in HI from Heiles & Troland (2005), in low-mass dense cores and molecular clouds in OH and in star-forming regions from CN (Crutcher 1999, Falgarone et al. 2008). The results of the Bayesian analysis performed on the ensemble of Zeeman measurements are the following,

1 - There is no increase of the magnetic field intensity up to gas densities $n_{\text{H},0} \sim 300 \text{ cm}^{-3}$, and above this threshold the observed values are consistent with an upper value increasing as $B_{\text{tot}} \propto n_{\text{H}}^{\kappa}$ with $\kappa \approx 0.65$. This change of behavior occurs at $N_{\text{H}} \sim 3 \times 10^{21} \text{ cm}^{-2}$, where clouds start to be self-gravitating.

2 - The sharp increase of the *upper limit of the magnetic field* with density above

$n_{\text{H},0} \sim 300 \text{ cm}^{-3}$ and the large scatter of the data have no straightforward interpretation, given the small number of data points. These results do not seem to support the model of star-formation controlled by gravity-driven ambipolar diffusion.

3 - The line drawn on Fig. 13 (right) corresponds to the critical mass-to-flux ratio $(M/\Phi)_{\text{crit}} = 3.5 \times 10^{-21} N_{\text{H}}/B_{\text{tot}}$. Therefore all the Zeeman measurements in molecular cloud cores, whether they are low-mass dense cores (OH) or high-mass dense cores and star-forming regions (CN), show that the mean mass-to-flux ratio $M/\Phi \sim 2$ to $3 \times (M/\Phi)_{\text{crit}}$. Thus, none of the molecular cloud cores observed so far have subcritical M/Φ .

4 - The turbulent and magnetic energies in all these clouds, including star-forming regions, are in approximate equipartition.

Sensitive OH Zeeman measurements performed in the core and envelope of four dark clouds by Crutcher et al. (2009) provide a mass-to-flux ratio smaller in the cores than in the envelopes, $(M/\Phi)_{\text{core}} < (M/\Phi)_{\text{env}}$. It is a provocative result, although close to the detection limit, because it is the opposite of the prediction of the ambipolar diffusion theory. Lazarian et al. (2012) propose that a process they term “reconnexion diffusion” efficiently removes magnetic flux from the turbulent envelopes of molecular clouds. However, the uncertainties and difficulties at measuring the magnetic field intensity make any definite conclusion likely premature.

6 Openings

All along this review, emphasis has been put on the importance of turbulence and magnetic fields on the physics of molecular clouds. Here, we would like to address, as openings, two related issues for which the dynamics of molecular cloud is crucial. First, we address the inter-relation between turbulence and chemistry. Indeed, while turbulence can drive chemistry by inducing high temperatures in dissipation bursts, chemistry helps to study the velocity field. Second, we present some theories that have been proposed to explain the star-formation rate in molecular clouds.

6.1 Link between chemistry and turbulence

6.1.1 Warm H_2 glitters of the cold ISM

We have seen that the turbulent energy density of molecular clouds is of the same order as the gravitational energy at large scale. One question has not been addressed yet: how is this huge energy dissipated, and where? Do we have any signpost of dissipation? The answer is probably positive: we may be witnessing turbulent dissipation in the recently discovered H_2 pure rotational emission of diffuse molecular clouds and in their remarkable molecular richness.

Cold H_2 cannot be detected in emission due to the symmetry and small moment of inertia of the molecule. Its lowest lying rotational levels have so large energies² that it precludes the detection of even the first pure rotational transitions of H_2 in environments devoid of UV radiation or shock excitation. By detecting the lowest

² The first excited levels of ortho- and para- H_2 lie at 510K ($J = 2$) and 1020K ($J = 3$), respectively, above the ground states $J = 0$ and $J = 1$

rotational lines of H₂ at an unexpected level in cold diffuse environments, *ISO-SWS* has challenged the traditional view of the ISM and disclosed the transient existence of tiny fractions of warm gas, disseminated within the cold ISM, but warm enough to excite these lines (Falgarone et al. 2005). The H₂ line emission has since then been observed by *Spitzer/IRS* in one edge of the Taurus molecular complex (Goldsmith et al. 2010) and in high-latitude clouds (Ingalls et al. 2011). The detected amounts of warm H₂ (*i.e.* in rotational levels $J \geq 2$ of the ground vibrational level) cannot be explained by the known sources of excitation in these environments. The existence of a few percent of warm molecular gas mixed with the cold diffuse ISM is not only inferred from these observations. H₂ absorption lines observed by FUSE, in the direction of late B stars probe a similar fraction of warm H₂ embedded in the cold diffuse ISM (Gry et al. 2002, Lacour et al. 2005). Similarly, the excess of H₂ rotational line emission in photo-dissociation regions (PDRs) with low UV-irradiation (Habart et al. 2011) calls for an additional heating mechanism.

A possible source of heating comes from the bursts of dissipation of supersonic turbulence which pervades the whole ISM. It is because the dissipation of turbulence is intermittent that the *local* gas heating is large enough to excite the H₂ pure rotational lines by collisions. These space-time bursts are modeled as low-velocity MHD shocks (Flower & Pineau des Forêts 1998, Lesaffre et al. 2012) and/or thin coherent vortices temporarily heating a small fraction of the gas ($\approx 1\%$) to temperatures up to 10^3 K (Joulain et al. 1998, Godard et al. 2009). The heated gas eventually cools down once the dissipation burst is over.

6.1.2 Need for alternative routes for molecule formation in diffuse unshielded environments

Molecular lines, and CO lines in particular, are major coolants of molecular clouds at high densities (Goldsmith & Langer 1978) while the fine-structure line of C⁺ (and to a lesser extent OI) dominates the cooling of diffuse molecular gas. On average, in the galactic plane, C⁺ cooling exceeds by far all the other coolants, as first shown by the *COBE* submillimeter all-sky survey (Bennett et al. 1994). At high latitude there is an excellent correlation of the C⁺ cooling rate with neutral atomic hydrogen, $\Lambda(\text{C}^+) = 2.6 \times 10^{-26} \text{ erg s}^{-1} \text{ H}^{-1}$. Chemistry is therefore a key issue in the understanding of the evolution of molecular clouds. The many unsolved issues, *i.e.* the unexpected molecular richness of the diffuse gas, its large (and highly fluctuating) CO abundances, to name a few, are indicators that some aspects of the cloud chemistry have been overlooked.

State-of-the-art models of photo-dominated regions (PDR) (Le Petit et al. 2006) have met with success even with uniform density distributions. Some species, like CH, have observed behaviours that are fully consistent with models predictions. But noteworthy discrepancies exist. Recently, outputs of numerical simulations of MHD turbulence (Hennebelle et al. 2008) have been used to compute the propagation of the UV radiation, the gas temperature and the chemistry in a self-consistent manner (Levrier et al. 2012). The average molecular abundances of H₂, CO, CN, CS are increased by a factor of a few, in better agreement with observations. But CO abundances remain below the observed values by about a factor of 10 for H₂ column densities in the range from a few $\times 10^{19}$ to 10^{21} cm^{-2} .

In standard chemistry, CO forms rapidly by reaction of C^+ with OH and H_2O and is photo-dissociated by UV photons. As H_2 , CO self-shields because its photo-dissociation proceeds via absorption in its own electronic transitions (van Dishoeck & Black 1988). OH and H_2O form via reactions of H_3^+ with oxygen. H_3^+ results from the ionization of hydrogen by cosmic rays followed by reaction with H_2 . Quoting Glassgold & Langer (1975), “When C^+ recombines in a gas rich in H_2 , it does not produce neutral carbon but directly CO”. The computation of the $C^+/C/CO$ transition, as well as the H/H_2 transition, is still a challenge to theorists. In steady-state chemistry, H_3^+ plays a pivotal role.

There is another route to CO that proceeds via highly endoenergetic reactions. This is why it has been overlooked in the chemistry of cold molecular clouds. It is initiated with the formation of CH^+ via $C^+ + H_2$ ($\Delta E/k = 4940K$), by rapid hydrogenations of CH^+ that produces CH_2^+ and CH_3^+ . This chain stops at CH_3^+ which becomes the pivotal cation of the “warm” chemistry by reacting with O to form HCO^+ the main source of CO through dissociative recombination.

The TDR model (for Turbulent Dissipation Regions, Godard et al., 2009) is based on the fact that turbulent dissipation that involves $\nabla \cdot \mathbf{v}$ and $\nabla \times \mathbf{v}$ is an intermittent quantity. The free parameters of the model are constrained by the known large-scale properties of turbulence (Joullain et al. 1998). In this model, the dissipation is due to both viscous dissipation and ion-neutral friction induced by the decoupling of the ionized and neutral flows in the central regions. Since the diffuse medium has a low density, its chemical and thermal inertia are large. A random line of sight through the medium therefore samples actively dissipating regions, relaxation phases, and the ambient medium. The chemical relaxation times of molecular species cover a broad range, from 200 yr for CH^+ up to 5×10^4 yr for CO. This introduces a potential complexity in the comparison of the observed abundances of different species.

The main successes of the TDR model are:

- the agreement of CH^+ and SH^+ observations with model predictions. SH^+ has even a larger formation endothermicity than CH^+ , via $S^+ + H_2$, ($\Delta E/k = 9860K$) (Menten et al. 2011, Godard et al. 2012);
- the scaling of CH^+ abundances with the turbulent dissipation rate;
- the H_2 pure rotational line emission of diffuse molecular gas (see previous section);
- the CO abundance of diffuse molecular gas.

An interesting properties of these models is that a fraction as small as a few per cent of warm gas, heated by the dissipation of turbulent energy, is sufficient to reproduce the observed H_2 line intensities, and their line ratios, as well as the abundances of specific molecules. These tend to be in better agreement with low rates-of-strain, *i.e.* models in which dissipation is dominated by ion-neutral friction. Finally, models of low velocity C-shocks with shock velocities in the range 5 to 8 km s⁻¹ have very similar chemical outputs (Lesaffre et al. 2012).

6.2 Role of density PDF for the star-formation rate (SFR)

Below we emphasize the importance of the density PDF regarding one of the most fundamental problems related to the formation of stars namely the star-formation rate. Various authors (namely Krumholz & McKee 2005, Padoan & Nordlund 2011,

Hennebelle & Chabrier 2011) have been recently proposing analytical theories that predict the star-formation rate within molecular clouds. The dimensionless *star-formation rate per free-fall time*, SFR , which has been introduced by Krumholz & McKee (2005) is the fraction of cloud mass converted into stars per cloud *mean* free-fall time, τ_{ff}^0 , *i.e.* $SFR = \frac{\dot{M}_*}{M_c} \tau_{ff}^0$. In this expression \dot{M}_* denotes the *total star-formation rate* arising from a cloud of mass M_c , size L_c and mean density ρ_0 .

As the physical ideas behind these theories are similar and relatively straightforward, though the results may differ significantly, we start with a general description. Considering a cloud with a density distribution, \mathcal{P} , close to the expression stated by Eq. (3): the densest parts will collapse in a few free-fall times if they are dense enough. This suggests that the star-formation rate could be simply estimated by summing over the density PDF up to some threshold, ρ_{crit} , and dividing by a few free-fall times, $\phi_t \tau_{ff}$, and multiplied by some efficiency $\epsilon \simeq 1/3 - 1.2$ that takes into account the fact that only a fraction of the mass initially within cores eventually ends up into stars (Matzner & McKee 2000, Ciardi & Hennebelle 2010). Thus, $SFR = \epsilon \int_{\delta_{crit}}^{\infty} (\tau_{ff}^0 / (\tau_{ff}(\rho) \phi_t)) (\rho / \rho_0) \mathcal{P}(\delta) d\delta$, where $\delta_{crit} = \ln(\rho_{crit} / \rho_0)$. The differences between the various estimates available in the literature reside mainly in the choice of ρ_{crit} and of the free-fall time.

The first theory along this line has been proposed by Krumholz & McKee (2005). In their approach, ρ_{crit} is determined from the condition that the corresponding Jeans length must be equal to the sonic length, λ_s , *i.e.* the length at which the velocity dispersion is equal to the sound speed. The underlying assumption is that turbulent support will be too efficient to enable star-formation at scales larger than the sonic length. This yields $\rho_{crit, KM} = \rho_0 (\phi_x \lambda_{J0} / \lambda_s)^2$, where ϕ_x is a coefficient of order unity, λ_{J0} is the Jeans length at the mean cloud density. Furthermore, they assume that the relevant free-fall time, $\tau_{ff}(\rho)$, is equal to the cloud mean free-fall time τ_{ff}^0 . Thus, they obtain a star-formation rate of the order of few percents.

Padoan & Nordlund (2011) make different choices regarding the critical density and the free-fall time. For the former they assume that it is obtained by requiring that the corresponding Jeans length is equal to the typical thickness of the shocked layer, inferred by combining isothermal shock jump conditions and the turbulent velocity scaling, $v \propto l^{0.5}$. This yields $\rho_{crit, PN} \simeq 0.067 \theta^{-2} \alpha_{vir} \mathcal{M}^2 \rho_0$, where $\theta \approx 0.35$ and α_{vir} is the virial parameter, $\alpha_{vir} = 2E_{kin} / E_{grav} = 5V_0^2 / (\pi G \rho_0 L_c^2)$, where V_0 is the rms velocity within the cloud, representative of the level of turbulent vs. gravitational energy in the cloud. To estimate the free-fall time, they compute its value at the critical density. This leads to a factor $\tau_{ff}^0 / \tau_{ff}(\rho_{crit}) = (\rho_{crit} / \rho_0)^{1/2}$ which is *independent* of the density. The SFR obtained in this way is about 3-10 times higher than what has been inferred by Krumholz & McKee. Moreover the dependence of the SFR on the Mach number at a given value of the virial parameter α is different. The SFR increases with the Mach number in the Padoan & Nordlund model, while it decreases according to Krumholz & McKee.

Hennebelle & Chabrier (2011) proceed differently. First, they infer a star-formation rate by a direct integration over the core mass spectrum derived by Hennebelle & Chabrier weighted by $\phi_t \tau_{ff}$, where τ_{ff} is the free-fall time associated to the core. It can be shown that the typical crossing time, at the scale of the core progenitor under the assumption that it is virialised and irre- spectively of the scale, is about 3 times the free-fall times. Therefore $SFR =$

$\rho_0^{-1} \int_0^{M_{cut}} \tau_{ff}^0 / \tau_{ff} M dN/dM(M) dM$ where M_{cut} is the core mass until which the integration must be performed. In the general case, this integral cannot be converted into a density integral of the kind obtained by Krumholz & McKee (2005) and Padoan & Nordlund (2011) mainly because of the scale dependence of the density PDF³. The physical reason is that an integral over the density only, does not take into account the spatial distribution. Indeed, one could construct a medium with a density PDF identical to the one observed in molecular clouds but with a very clumpy gas spatial distribution such that all clumps would have a mass smaller than the Jeans mass. In this case, no star could form by gravitational collapse. However, if the gas distribution is sufficiently regular, as it is the case for density structures generated by turbulence (appendix B of Hennebelle & Chabrier 2008), then the SFR can be written as an integral of the density field and it is not necessary to take the detail of the spatial distribution into account.

As it is clear from the last SFR expression, the density PDF should be weighted by the local free-fall time when performing the integration over the density to get the SFR. Estimating the free-fall time at the mean cloud density or at the critical density, leads to overestimate the free-fall time in the densest regions and therefore underestimate the SFR. When the free-fall time is kept inside the integral, as it should, the following expression for the SFR is obtained:

$$\begin{aligned} SFR &= \epsilon \int_{\delta_{crit}}^{\infty} \frac{\tau_{ff}^0}{\tau_{ff}(\rho) \phi_t} \frac{\rho}{\rho_0} \mathcal{P}(\delta) d\delta = \frac{\epsilon}{\phi_t} \int_{\delta_{crit}}^{\infty} \left(\frac{\rho}{\rho_0} \right)^{3/2} \mathcal{P}(\delta) d\delta \\ &= \frac{\epsilon}{2\phi_t} \exp(3\sigma_0^2/8) \left[1 + \operatorname{erf} \left(\frac{\sigma_0^2 \ln(\rho_{crit}/\rho_0)}{2^{1/2}\sigma_0} \right) \right], \end{aligned} \quad (13)$$

where ρ_{crit} is the critical density.

Comparing the various models, Hennebelle & Chabrier (2011) conclude (their figure 1) that the choice of Krumholz & McKee (2005) to estimate the free-fall time as the mean cloud free-fall time, leads to underestimate the SFR by almost one order of magnitude. On the other hand, the choice of Padoan & Nordlund (2011) to estimate the free-fall time at the critical density leads to underestimate the SFR by a factor 2-3. The choice of the critical density has also some impact and leads to SFR that vary by a factor of the order of 3. Direct comparisons with SFR inferred from observations (e.g. Heiderman et al. 2010, Kennicutt and Evans, 2012) have been performed but given the relatively large scatter of the data, it seems hard to draw firm conclusions. Once the dependence on the free-fall time is properly taken into account, all model predictions are in comparable agreement with the molecular cloud data. Moreover, the theoretical predictions are all hampered by large uncertainties due to the parameters ϵ , ϕ_t but also the value of the critical density up to which the integration is performed.

7 The road ahead

This review has stressed the role played by turbulence in the physics of molecular clouds. As the whole field of turbulence, including incompressible turbulence and

³ More precisely, this is expressed by the second term of the right hand side of Eq. (33) of Hennebelle & Chabrier (2008) that we do not write here for conciseness

ideal MHD turbulence, remains a challenge to physicists, unraveling interstellar turbulence is an even greater task because it is compressible and magnetized, and it entails complicated non-ideal MHD processes, radiative cooling, and interplay with self-gravity. Moreover, the lesson drawn from observations is that the range of scales coupled by interstellar turbulence likely extends from AU-scales, close to the mean free path of atoms and molecules, to galactic scales. Two facets are therefore particularly challenging for the future, on observational and theoretical grounds: (1) a better knowledge of interstellar turbulence and the nature of its dissipation processes; (2) the respective impact of the large scale environment and the star-formation feedback upon the evolution of star-forming clouds.

Several aspects of interstellar turbulence are particularly relevant to our understanding of molecular clouds. First, the density PDF is largely determining the SFR and the CMF. A better theoretical knowledge of its dependence on the Mach number and on the adiabatic index, would lead to more quantitative predictions of the SFR and CMF. Second, the nature of the dissipation structures and the local heating induced by turbulent dissipation, may be a clue to explain the abundance of some chemical species. In turn, the observations of these species will provide reliable diagnostics to help constraining the dynamics of the flows. Third, the origin of the filaments observed in molecular clouds and the role they play in their evolution as well as in the star-formation process remain speculative. Finally, the coupling between the magnetic field and the gas in presence of turbulence is only partially understood (e.g. Santos-Lima et al. 2012).

As amply emphasized, molecular clouds continue to accrete during a long period of their lifetime. At some stage, when the gas has formed enough stars, stellar feedback becomes important and even dominant, possibly disrupting the cloud and setting the star-formation efficiency at the observed low level. The different phases of this scenario need to be assessed and quantified, in particular the duration as well as the amount of energy which is released inside the cloud from the various sources. While it seems unavoidable that dense cloud formation involves converging/colliding flows, the nature of these flows remains largely open and important questions are still unsolved such as: What drives them ? What is the amount of mass they deliver ? What is their geometry ? Are stars forming while the cloud is still growing in mass? Concerning feedback, it is not clear which process is dominant and which scales are affected.

In conclusion, in spite of significant progress, the old controversy of what is regulating star-formation within molecular clouds, magnetic fields, turbulence or feedback, is still largely present and unsolved. Likely the three factors play a significant role and contribute to determine the outcome of star-formation.

8 Acknowledgement

This review is dedicated to the masters that opened the field in the early 1970s, Pat Thaddeus, Phil Solomon and Tom Phillips on the observations side and George Field on the theory side. We thank Alexei Kritsuk, Fred Lo, Frédéric Bournaud, Maryvonne Gerin, Pierre Lesaffre and Leo Blitz for a critical reading of the manuscript and for suggestions which have improved it.

References

1. Abdo, A.A. Ackermann, M., Ajello, M. et al., 2010, ApJ, 710, 133
2. Abergel, A., Boulanger, F., Mizuno, A., Fukui, Y., 1994, ApJ, 423, L59
3. Ackermann, M. Ajello, M., Baldini, L. et al. 2011, ApJ, 726, 81
4. Alvés, J., Lombardi, M. & Lada, C., 2007, A&A, 462, L17
5. André, P., Men'shchikov, A., Bontemps, S. et al. A&A, 2010, 518, L102
6. André, P., Men'shchikov, A., Könyves, V., Arzoumanian, D., 2011, IAUS, 270, 255
7. Anselmet, F., Antonia, R., Danaila, L., 2001, P&SS, 49, 1177
8. Arzoumanian, D., André, Ph, Didelon, P. et al., 2011, A&A, 529, L6
9. de Avillez M., Breitschwerdt D., 2005, A&A 436, 585
10. Audit E., Hennebelle P., 2005, A&A 433, 1
11. Audit E., Hennebelle P., 2010, A&A, 511, 76
12. Ballesteros-Paredes, J., Hartmann, L., Vázquez-Semadeni, E., 1999, ApJ, 527, 285
13. Bally, J., Lanber, W., Stark, A., Wilson, R., 1987, ApJ, 312, L45
14. Bally, J., Aguirre J., Battersby C. et al. 2010, ApJ, 721, 137
15. Banerjee, R., Vázquez-Semadeni, E., Hennebelle, P., Klessen, R., 2009, MNRAS, 398, 1082
16. Barriault, L., Joncas, G., Falgarone, E. et al., 2010, MNRAS, 406, 2713
17. Basu, S., 2000, ApJ, 540, L103
18. Basu, S., Ciolek, G. 2004, ApJ, 607, L39
19. Basu, S., Mouschovias, T. 1995, ApJ, 452, 386
20. Bayly, B., Levermore, C., Passot, T., 1992, PhFl, 4, 945
21. Bec, J., Frisch, U., 2000, PhRvE, 61, 1395
22. Begum, A., Stanimirovic, S., Goss, W., Heiles, C., Pavkovich, A., Hennebelle, P., 2010, ApJ, 725, 1779
23. Benjamin, R., Churchwell, E., Babler, B., 2003, PASP, 115, 953
24. Bennett, C., Fixsen, D., Hinshaw, G. et al. 1994, ApJ, 434, 587
25. Bensch, F., Stutzki, J., Ossenkopf, V., 2001, A&A, 366, 636
26. Beresnyak, A., Lazarian, A., Cho, J., 2005, ApJ, 624, L93
27. Beresnyak, A., 2011, PhRvL, 106, 5001
28. Bertoldi, F., McKee, C., 1992, ApJ, 395, 140
29. Biskamp, D., 2003, *Magneto-hydrodynamic turbulence*, matu.book
30. Blaisdell, G, Mansour, N., Reynolds, W., 1993, JFM, 256, 443
31. Blitz, L. & Shu F.H., 1980, ApJ, 238, 148
32. Blitz, L. & Thaddeus, P., 1980, ApJ, 241, 676
33. Blitz, L., Rosolowsky, E., 2004, ApJ, 612, L29
34. Blitz, L., Rosolowsky, E., 2006, ApJ, 650, 933
35. Boldyrev, S., Nordlund, A., Padoan, P., 2002, ApJ, 573, 678
36. Boldyrev, S., 2005, ApJ, 626, L37
37. Bond, J., Cole, S., Efstathiou, G., Kaiser, N., 1991, ApJ, 379, 440
38. Bonazzola, S., Heyvaerts, J., Falgarone, E., Pérault, M., Puget, J. L., 1987, A&A, 172, 293
39. Bournaud, F., Elmegreen, B., Teyssier, R., Block, D., Puerai, I., 2010, MNRAS, 409, 1088
40. Brunt, C., Heyer, M., MacLow, M.-M., 2009, A&A, 504, 883
41. Burkhart, B., Falceta-Gonçalves, D. Kowal, G., Lazarian, A., 2009, ApJ, 693, 250
42. Chabrier, G., 2003, PASP, 115, 763
43. Chabrier, G., Hennebelle, P., 2010, ApJ, 725, L79
44. Chandrasekhar, S., Fermi, E., 1953, ApJ, 118, 116
45. Chapman, N., Goldsmith, P., Pineda, J. et al. 2011, ApJ, 741, 21
46. Chièze, J.-P., 1987, A&A, 171, 225
47. Cho, J., Lazarian, A., Vishniac, E., 2002, ApJ, 564, 291
48. Ciardi, A., Hennebelle, P., 2010, MNRAS, 409, L39
49. Clemens, D., Sanders, D., Scoville, N., Solomon, P., 1986, ApJS, 60, 297
50. Cox, D., 2005, ARA&A, 43, 337
51. Crutcher, R., 1999, ApJ, 520, 706
52. Crutcher, R., Wandelt, B., Heiles, C., Falgarone, E., Troland, T., 2010, ApJ, 725, 466
53. Crutcher, R., Hakobian, N., Troland, T., 2009, ApJ, 692, 844
54. Curry, C., 2000, ApJ, 541, 831
55. Dame, T., Ungerechts, H., Cohen, R. et al. 1987, ApJ, 322, 706
56. Dame, T., Hartmann, D., Thaddeus, P., 2001, ApJ, 597, 792
57. Dame, T., Thaddeus, P., 1994, ApJ, 436, L173

58. Deshpande, A., Dwarakanath, K., Goss, W., 2000, ApJ, 543, 227
59. Dib, S., Brandenburg, A., Kim, J., Gopinathan, M., André, P., 2008, ApJ, 678, L105
60. Dobbs, C., Bonnell, I., 2007, MNRAS, 376, 1747
61. Downes, T., o'Sullivan, S., 2009, ApJ, 701, 1258
62. Dubrulle, B., 1994, PhRvL, 73, 959
63. Dutrey, A., Duvert, G., Castest, A., Langer, W., Bally, J., Wilson, R., 1991, A&A, 247, L9
64. Egan, M., Shipman, R., Price, S. et al. 1998, ApJ, 494, L199
65. Egusa, F., Koda, J., Scoville, N., 2011, ApJ, 726, 85
66. Elmegreen, B., Elmegreen, D., 1987, ApJ, 320, 182
67. Elmegreen, B., Falgarone, E., 1996, ApJ, 471, 816
68. Elmegreen, B., Kim, S., Staveley-Smith, L., 2001, ApJ, 548, 749
69. Elmegreen, B., Scalo, J., 2004, ARA&A, 42, 211
70. Falgarone, E., Puget, J.-L., 1985, A&A, 142, 157
71. Falgarone, E., Puget, J.-L., 1986, A&A, 162, 235
72. Falgarone, E., Phillips, T., Walker, C., 1991, ApJ, 378, 186
73. Falgarone, E., Puget, J.-L., Péroult, M., 1992, A&A, 257, 715
74. Falgarone, E., Pety, J., Phillips, T., 2001, ApJ, 555, 178
75. Falgarone, E., Hily-Blant, P., Levrier, F., 2004, Ap&SS, 292, 285
76. Falgarone, E., Verstraete, L., Pineau Des Forêts, G., Hily-Blant, P., 2005, A&A, 433, 997
77. Falgarone, E., Troland, T., Crutcher, R., Paubert, G., 2008, A&A, 487, 247
78. Falgarone, E., Pety, J., Hily-Blant, P., 2009, A&A, 507, 355
79. Falgarone, E., Ossenkopf V., Gerin M. et al. 2010, A&A, 518, L118
80. Falgarone, E., Godard, B., Cernicharo, J. et al. 2010, A&A, 521, L15
81. Federrath, C., Klessen, R., Schmidt, W., 2008, ApJ, 688, L79
82. Federrath, C., Klessen, R., Schmidt, W., 2009, ApJ, 692, 364
83. Federrath, C., Roman-Duval, J., Klessen, R., Schmidt, W., Mac Low, M.-M., 2010, A&A, 512, 81
84. Fischera, J., Martin, P., 2012, A&A, 542, 77
85. Fiege, J., Pudritz, R., 2000a, MNRAS, 311, 85
86. Fiege, J., Pudritz, R., 2000b, ApJ, 544, 830
87. Field G., Goldsmith D., Habing H., 1969, ApJ, 155, 149
88. Field, G., Blackman, E., Keto, E., 2008, MNRAS, 385, 181
89. Field, G., Blackman, E., Keto, E., 2011, MNRAS, 416, 710
90. Fitzpatrick, E., Spitzer, L., 1997, ApJ, 427, 232
91. Fleck, R., 1996, ApJ, 458, 739
92. Flower, D., Pineau des Forêts, G., 1998, MNRAS, 297, 1182
93. Frisch, U., 1996, *Turbulence*, turb.book
94. Fukui, Y., Kawamura, A., Wong, T. et al. 2009, ApJ, 705, 144
95. Galtier, S., Banerjee, S., 2011, PhRvL, 107, 4501
96. Gautier, T., Boulanger, F., Péroult, M., Puget, J.-L., 1992, AJ, 103, 1313
97. Gazol A., Vázquez-Semadeni E., Sánchez-Salcedo F., Scalo J., 2001, ApJ 557, L124
98. Gazol A., Vázquez-Semadeni E., Kim J., 2005, ApJ 630, 911
99. Gerin, M., de Luca, M., Goicoechea, J. et al., 2010, A&A, 521, L16
100. Glassgold, A., Langer, W., 1975, ApJ, 204, 403
101. Glover, S., Mac Low, M., 2007, ApJS, 169, 239
102. Glover, S., Clark, P., 2012, MNRAS, 421, 9
103. Godard, B., Falgarone, E., Pineau des Forêts, G., 2009, A&A, 495, 847
104. Godard, B., Falgarone, E., Gerin, M., et al. 2012, A&A, 540, 87
105. Goldbaum, N., Krumholz, M., Matzner, C., McKee, C., 2011, ApJ, 738, 101
106. Goldreich, P., Sridhar, S., 1995, ApJ, 438, 763
107. Goldsmith, P., Langer, W., 1978, ApJ, 222, 881
108. Goldsmith, P., Heyer, M., Narayanan, G., Snell, R., Li, D., Brunt, C., 2008, ApJ, 680, 1132
109. Goldsmith, P., Velusamy, T., Li, D., Langer, W., 2010, ApJ, 715, 1370
110. Gratier, P., Braine, J., Rodriguez-Fernandez, N. et al. 2010, A&A, 522, 3
111. Gratier, P., Braine, J., Rodriguez-Fernandez, N. et al. 2012, A&A, 542, 108
112. Grenier, I., Casandjian, J.-M., Terrier, R., 2005, Sci, 307, 1292
113. Gritschneider, M., Naab, T., Walch, S., Burkert, A., Heitsch, F., 2009, ApJ, 694, L26
114. Gry, C., Boulanger, F., Nehmé, C., Pineau des Forêts, G., Habart, E., Falgarone, E., 2002, A&A, 391, 675

114. Habart, E., Abergel, A., Boulanger, F. et al., 2011, *A&A*, 527, 122
115. Hartmann, J., 1904, *ApJ*, 19, 268
116. Hartmann, L., 2002, *ApJ*, 578, 914
117. Hasegawa, T., Sato, F., Fukui, Y., 1983, *AJ*, 88, 658,
118. Haud, U., Kalberla, P., 2007, *A&A*, 466, 555
- heiderman. Heiderman, A., Evans, N., Allen, L., Huard, T., Heyer, M., 2010, *ApJ*, 723, 1019
119. Heiles, C., 2000, *AJ*, 119, 923
120. Heiles, C., Troland, T., 2003, *ApJ*, 586, 1067
121. Heiles, C., Troland, T., 2005, *ApJ*, 624, 773
- Heithausen et al. 1998. Heithausen, A., Bensch, F., Stutzki, J., Falgarone, E., Panis, J.-F., 1998, *A&A*, 331, L65
122. Heithausen, A., 2002, *A&A*, 393, L41
123. Heithausen, A., Bertoldi, F., Bensch, F. et al., 2002, *A&A*, 383, 591
124. Heithausen, A., 2004, *A&A*, 606, L13
125. Heithausen, A., 2006, *A&A*, 450, 193
126. Heitsch F., Burkert A., Hartmann L., Slyz A., Devriendt J., 2005, *ApJ*, 633, 113
127. Heitsch F., Slyz A., Devriendt J., Hartmann L., Burkert A., 2006, *ApJ*, 648, 1052
128. Heitsch F., Hartmann L., Slyz A., Devriendt J., Burkert A., 2008, *ApJ*, 674, 316
129. Heitsch F., Ballesteros-Paredes, Hartmann L., 2009, *ApJ*, 704, 1735
130. Hennebelle P. & Pérault M., 1999, *A&A*, 351, 309
131. Hennebelle P. & Pérault M., 2000, *A&A*, 359, 1124
132. Hennebelle, P., Pérault, M., Teyssier, D., Ganesh, S., 2001, *A&A*, 365, 598
- Hennebelle & Audit 2007. Hennebelle, P., Audit, E., 2007, *A&A*, 465, 431
- Hennebelle & Chabrier 2008. Hennebelle, P., Chabrier, G., 2008, *ApJ*, 684, 395
133. Hennebelle, P., 2012, *A&A*, 545, 147
134. Hennebelle, P., Banerjee, R., Vázquez-Semadeni, E., Klessen, R., Audit, E., 2008, *A&A*, 486, L43
- Hennebelle & Chabrier 2011. Hennebelle, P., Chabrier, G., 2011, *ApJ*, 743, L29
135. Herrera, C.N., Boulanger, F., Nesvadba, N., 2011, *A&A*, 534, 138
136. Herrera, C.N., Boulanger, F., Nesvadba, N., Falgarone, E. 2012, *A&A*, 538, L9
137. Heyer, M., Carpenter, J., Snell, R., 2001, *ApJ*, 551, 852
138. Heyer, M., Brunt, C. 2004, *ApJ*, 615, L45
139. Heyer, M., Gong, H., Ostriker, E., Brunt, C. 2008, *ApJ*, 680, 420
140. Heyer, M., Krawczyk, C., Duval, J., Jackson, J., 2009, *ApJ*, 699, 1092
141. Heyer, M., Brunt, C. 2012, *MNRAS*, 420, 1562
142. Hildebrandt, R., Kirby, L., Dotson, J., Houde, M., Vaillancourt, J., 2009, *ApJ*, 696, 567
143. Hily-Blant, P., Falgarone, E., Pety, J. 2008, *A&A*, 481, 367
144. Hily-Blant, P., Falgarone, E., 2009, *A&A*, 500, L59
145. Hopkins, P., Quataert, E., Murray, N., 2011, 417, 950
146. Hopkins, P., *MNRAS*, 2012a, 423, 2016
147. Hopkins, P., *MNRAS*, 2012b, 423, 2037
148. Houde, M., Vaillancourt, J., Hildebrand, R., Chitsazzadeh, S., Kirby, L., 2009, *ApJ*, 706, 1504
149. Hughes, A., Wong, T., Ott, J. et al. 2010, *MNRAS*, 406, 2065
150. Ingalls, J., Bania, T., Boulanger, F., Draine, B., Falgarone, E., Hily-Blant, P., 2011, *ApJ*, 743, 174
151. Inoue, T., Yamazaki, R., Inutsuka, S.-i., 2009, *ApJ*, 695, 825
152. Inoue, T., Inutsuka, S.-I., 2012, *ApJ*, 759, 35
153. Inutsuka, S.-I., and Miyama S., 1992, *ApJ*, 388, 392
154. Iroshnikov, P., 1963, *Sov. Astron.*, 7, 566,
155. Jackson, J., Rathborne, J., Shah, R. et al., 2006, *ApJS*, 163, 145
156. Jackson, J., Finn, S., Chambers, E., Rathborne, J., Simon, R., 2010, *ApJ*, 719, L185
157. Jenkins, E., Tripp, T., 2011, *ApJ*, 734, 65
158. Johnstone, D., Wilson, C., Moriarty-Schieven, G., Joncas, G., Smith, G., Gregersen, E., Fich, M., 2000, *ApJ*, 545, 327
159. Joulain, K., Falgarone, E., Pineau des Forêts, Flower, D., 1998, *A&A*, 340, 241
160. Jung, R., Mac Low, M.-M., 2006, *ApJ*, 653, 1266
161. Kainulainen, J., Beuther, H., Henning, T., Plume, R., 2009, *A&A*, 508, L35
162. Kainulainen, J., Alves, J., Beuther, H., Henning, T., Schuller, F., 2011, *A&A*, 536, 48
163. Kawamura, A., Mizuno, Y., Minamidani, T. et al. 2009, *ApJS* 184, 1
164. Kennicutt, R., Evans, N.J., 2012, *ARA&A* 50, 531

165. Keto, E., Myers, P., 1986, ApJ, 304, 466
166. Kevlahan, N., Pudritz, R., 2009, ApJ, 702, 39
167. Klessen, R., 2000, ApJ, 635, 869
168. Klessen, R., Hennebelle, P., 2010, A&A, 520, 17
169. Kim, J., Ryu, D., 2005, ApJ, 630, L45
170. Koda, J., Scoville, N., Sawada, T., 2009, ApJ, 700, L132,
171. Kolmogorov A.N. 1941, Proc. R. Soc. London Ser. A 434, Reprinted in 1991
172. Koyama, H., Inutsuka S., 2000, ApJ 532, 980
173. Koyama, H., Inutsuka S., 2002, ApJ 564, L97
174. Koyama, H., Ostriker, E., 2009, ApJ, 693, 1346
175. Kraichnan, R. 1965, Phys. Fluids, 8, 1385,
176. Kramer, C., Stutzki, J., Rohrig, R., Corneliussen, U., 1998, A&A, 329, 249
177. Kritsuk, A., Norman, M., Padoan, P., Wagner, R., 2007, ApJ, 665, 416
178. Kritsuk A., Norman M., Wagner, R., 2011, ApJ, 727, L20
179. Kritsuk A., Norman M., 2011, arXiv1111.2827
180. Kroupa, P., 2002, Science, 295, 82
181. Krumholz, M., McKee, C., 2005, ApJ, 630, 250
182. Kunz, M., Mouschovias, T., 2009, ApJ, 399, L94
183. Lacour, S., Ziskin, V., Hébrard, G., Oliveira, C., André, M., Ferlet, R., Vidal-Madjar, A. 2005, ApJ, 627, 251
184. Lada, E., Evans, N., Falgarone, E., 1997, ApJ, 488, 286
185. Ladd, E., Myers, P., Goodman, A., 1994, ApJ, 433, 117
186. Larson, R., 1981, MNRAS, 194, 809
187. Larson, R., 1985, MNRAS, 214, 379
188. Lazarian, A., Pogosyan, D., 2000, ApJ, 537, 720
189. Lazarian, A., Hoang, D., 2007, ApJ, 669, L77
190. Lazarian, A., Esquivel, A., Crutcher, R., 2012, ApJ, 757, L154
191. Lebrun, F., Bennett, K., Bignani, G., et al. 1983, ApJ, 274, L231
192. Lemaster, N., Stone, J., 2008, ApJ, 682, L97
193. Lee, H.-H., Herbst, E., Pineau des Forêts, G., Roueff, E., Le Bourlot, J., 1996, A&A, 311, 690
194. Lee, E., Brachet, M.-E., Pouquet, A., Mininni, P., Rosenberg, D., 2010, PhRvE, 81, 6318L
195. Le Petit, F., Nehmé, C., Le Bourlot, J., Roueff, E., 2006, ApJS, 164, 506
196. Lesaffre, P., Pineau des Forêts, G., Godard, B. et al., 2012, A&A, *accepted*
197. Levrier, F., Le Petit, F., Hennebelle, P., Lesaffre, P., Gerin, M., Falgarone, E., 2012, A&A, 544, 22
198. Li, H., Griffin, G., Krejny, M., Novak, G., Loewenstein, R., Newcomb, M., Calisse, P., Chuss, D., 2006, ApJ, 648, 340
199. Li, D., Goldsmith, P., 2003, ApJ, 585, 823
200. Li, Z.-Y., Nakamura, F. 2005, ApJ, 631, 411
201. Li, P.S., McKee, C., Klein, R., Fisher, R., 2008, ApJ, 684, 380
202. Li, P.S., McKee, C., Klein, R., 2012, ApJ, 744, 732
203. Lin, C., Mestel, L., Shu, F., 1965, ApJ, 142, 1431
204. Lis, D., Pety, J., Phillips, T., Falgarone, E., 1996, ApJ, 463, L623
205. Liszt, H., Lucas, R., 1998, A&A, 339, 561
206. Liszt, H., Pety, J., Lucas, R., 2010, A&A, 518, 45
207. Liszt, H., Pety, J., 2012, A&A, 541, L58
208. Low, F., Young, E., Beintema, D. et al. 1984, ApJ, 278, L19
209. MacLow, M.-M., 1999, ApJ, 524, 169
210. MacLow, M.-M., Klessen, R., 2004, RvMP, 76, 125
211. Mason, J, Perez, J., Boldyrev, A., Cattaneo, F., 2012, PhPl, 19, 5902
212. Matthews, B., McPhee, C., Fissel, L., Curran, R., 2009, ApJS, 182, 143
213. Matzner, C., 2002, ApJ, 566, 302
214. Matzner, C.D. & McKee, C., 2000, ApJ, 545, 364
215. Maury, A., André, P., Li, Z.-Y., 2009, A&A, 499, 175
216. May, J., Bronfman, L., Alvarez, H., Murphy, D., Thaddeus, P., 1993, A&AS, 99, 105
217. May, J., Murphy, D., Thaddeus, P., 1988, A&AS, 73, 51
218. McKee, C.M., Ostriker, E., 2007, ARA&A, 45, 565
219. McKee, C.M., Li, P.S., Klein, R.I. 2010 ApJ 720, 1612
220. Menten, K., Wyrowski, F., Belloche, A., Güsten, R., Dedes, L., Müller, H., 2011, A&A, 525, 77

221. Mestel, L., Spitzer, L., 1956, MNRAS, 116, 503
222. Mininni, P., Pouquet, A., Montgomery, D., 2006, PhRvL, 97, 4503
223. Miville-Deschênes M.-A., Joncas G., Falgarone E., Boulanger F., 2003a, A&A 411, 109
224. Miville-Deschênes M.-A., Levrier, F., Falgarone E., 2003b, A&A 593, 831
225. Miville-Deschênes, M.-A., Martin, P., Abergel, A., 2010, A&A, 518, L104
226. Mizuno, A., Onishi, T., Yonekura, Y., Nagahama, T., Ogawa, H., Fukui, Y., 1995, ApJ, 445, L161
227. Moffatt, H., Kida, S., Ohkitani, K., 1994, JFM, 259, 241
228. Moisy, F., Jiménez, J., 2004, JFM, 513, 111
229. Molina, F., Glover, S., Federrath, C., Klessen, R., 2012, MNRAS, 423, 268
230. Motte, F., André, P., Neri, R., 1998, A&A, 336, 150
231. Mouschovias, T., Spitzer, L. 1976, ApJ, 210, 326
232. Mouschovias, T., Paleologou, E. 1981, ApJ, 246, 48
233. Müller, C., Biskamp, D., 2000, PhRvL, 84, 475
234. Myers P., 2009a, ApJ, 706, 1341
235. Myers P., 2009b, ApJ, 700, 1609
236. Nagai, T., Inutsuka, S.-I., Miyama, S., 1998, ApJ, 506, 306
237. Nakamura, F., Li, Z.-Y., 2007, ApJ, 662, 395
238. Neufeld, D., Goicoechea, J., Sonnentrucker, P., et al., 2010a, A&A, 521, L10
239. Neufeld, D., Sonnentrucker, P., Phillips, T., et al., 2010b, A&A, 518, L108
240. Ossenkopf, V., Mac Low, M.-M., 2002, A&A, 390, 307
241. Ostriker, J., 1964, ApJ, 140, 1056
242. Ostriker, E., Stone, J., Gammie, C., 2001, ApJ, 546, 980
243. Padoan, P., Nordlund, A., Jones, B., 1997, MNRAS, 288, 145
244. Padoan, P., Nordlund, A., 1999, ApJ, 526, 279
245. Padoan, P., Juvela, M., Goodman, A., Nordlund, A., 2001, ApJ, 553, 227
246. Padoan, P., Nordlund, A., Kritsuk, A., Norman, M., Li, P.-S., 2007, ApJ, 661, 972
247. Padoan, P., Nordlund, A., 2011, ApJ, 730, 40
248. Pan, L., Wheeler, J., Scalo, J., 2008, ApJ, 681, 470
249. Passot T., Vázquez-Semadeni E., 1998, Phys. Rev. E., 58, 4501
250. Passot T., Vázquez-Semadeni E., 2003, A&A, 398, 845
251. Penzias, A., Solomon, P., Jefferts, K., Wilson, R., 1972, ApJ, 174, L43
252. Pérault, M., Falgarone, E., Puget, J.-L., 1985, A&A, 152, 371
253. Pérault, M., Omont, A., Simon, G. et al. 1996, A&A, 315, L165
254. Peretto, N., Fuller, G., 2010, ApJ, 723, 555
255. Planck collaboration, Ade, P.A.R., Aghanim, N., Arnaud, M. et al., 2012, A&A, 536, A19
256. Politano, H., Pouquet, A., 1995, PhRvE, 52, 636
257. Porter, D., Pouquet, A., Woodward, P., 2002, PhRvE, 66, 6301
258. Press, W., Schechter, P., 1974, ApJ, 187, 425
259. Price, S., Egan, M., Carey, S., 2001, AJ, 121, 2819
260. Price, D., Bate, M., 2008, MNRAS, 385, 1820
261. Rathborne, J., Jackson, J., Chambers, E. et al. 2010, ApJ, 715, 310
262. Roman-Duval, J., Jackson, J., Heyer, M., Rathborne, J., Simon, R., 2010, A&A, 723, 492
263. Sakamoto, S., 2002, ApJ, 565, 1050
264. Sakamoto, S., Sumada, K., 2003, ApJ, 594, 340
265. Salpeter, E., 1955, ApJ, 121, 161
266. Sánchez-Salcedo F., Vázquez-Semadeni E., Gazol A., 2002, ApJ 577, 768
267. Sanders, D., Clemens, D., Scoville, N., Solomon, P., 1986, ApJS, 60, 1
268. Santos-Lima, R., de Gouveia Dal Pino, E., Lazarian, A., 2012, ApJ, 747, 21
269. Scalo J., Pumphrey, W. 1982, ApJ, 258, L29
270. Scalo, J., Elmegreen, B., 2004, ARA&A, 42, 275
271. Schmid-Burgk, J., 1967, ApJ, 149, 727
272. Schmidt, W., Federrath, C., Hupp, M., Kern, S., Niemeyer, J., 2009, A&A, 494, 127
273. Schmidt, W., Kern, S., Federrath, C., Klessen, R., 2010, A&A, 516, 25
274. Seifreid, D., Schmidt, W., Niemeyer, J. 2011, A&A, 526, 14
275. She, Z.-S., Leveque, E., 1994, Phys. Rev. 72, 336
276. She, Z.-S., Waymire, E., 1995, Phys. Rev. 74, 262
277. Shetty, R., Glover, S., Dullemond, C., Klessen, R., 2011, MNRAS, 412, 1686
278. Shu, F., 1977, ApJ, 214, 488
279. Shu, F. H., Adams, F. C., Lizano, S. 1987, ARA&A 25, 23
280. Slyz, A., Devriendt, J., Bryan, G., Silk, J., 2005, MNRAS, 356, 737

281. Smith, R., Clark, P., Bonnell, I., 2009, MNRAS, 396, 830
282. Solomon, P., Rivolo, A., Barrett, J., Yahil, A., 1987, ApJ, 319, 730
283. Sonnentrucker, P., González-Alfonso, E., Neufeld, D., 2007, ApJS, 168, 58
284. Sonnentrucker, P., Neufeld, D., Phillips, T., et al., 2010, A&A, 521, L12
285. Spitzer, L., 1978, *Physical processes in the interstellar medium*, ppim.book
286. Snow, T., McCall, B., 2006, ARA&A, 44, 367
287. Stanimirovic, S., Lazarian, A., 2001, ApJ, 551, L53
288. Stodólkiewicz, J., 1963, AcA, 13, 30
289. Stutzki, J., Bensch, F., Heithausen, A., Ossenkopf, V., Zielinsky, M., 1998, A&A, 636, 697
290. Sun, K., Kramer, C., Ossenkopf, V., et al., 2006, A&A, 451, 539
291. Swinbank, A., Smail, I., Longmore, S. et al., 2010, Natur, 464, 733
292. Tachihara, K., Mizuno, A., Fukui, Y., 2000, ApJ, 528, 817
293. Tasker, E., Tan, J., 2009, ApJ, 700, 358
294. Tassis, K., Christie, D., Urban, A. et al. 2010, MNRAS, 408, 1089
295. Testi, L., Sargent, A., 1998, ApJ, 508, L91
296. Tilley, D., Balsara, D., 2010, MNRAS, 406, 1201
297. Tremblin, P., Audit, E., Minier, V. et al., 2012, A&A, 546, 33
298. Ungerechts, H., Thaddeus, P., 1987, ApJS, 63, 645
299. van Dishoeck, E., Black, J., 1988, ApJ, 334, 771
300. Vázquez-Semadeni, E., 1994, ApJ, 423, 681
301. Vázquez-Semadeni, E., Passot, T., Pouquet, A., 1995, ApJ, 473, 881
302. Vázquez-Semadeni E., Ryu D., Passot T., González R., Gazol A., 2006, ApJ 643, 245
303. Vázquez-Semadeni, E., González, R., Ballesteros-Paredes, J., Adriana, G., Jongsoo, K., 2008, MNRAS, 390, 769
304. Vázquez-Semadeni, E., Banerjee, R., Gómez, G., Hennebelle, P., Duffin, D., Klessen, R., 2011, MNRAS, 414, 2511
305. Vestuto, J., Ostriker, E., Stone, J., 2003, ApJ, 590, 858
306. Walder R., Folini D., 1998, A&A, 330, L23
307. Wan, M., Oughton, S., Servidio, S., Matthaeus, W., 2012, JFM, 697, 296
308. Wang, P., Li, Z.-Y., Abel, T., Nakamura, F., 2010, ApJ, 709, 27
309. Wannier, P., Lichten, S., Morris, M., 1983, ApJ, 268, 727
310. Ward-Thompson, D., André, P., Crutcher, R., Johnstone, D., Onishi, T., Wilson, C., 2007, *Protostars & Planets V*, prpl.conf 33
311. Ward-Thompson, D., Kirk, J., André, P., 2010, A&A, 518, L92
312. von Weizsäcker, C, 1951, ApJ, 114, 165
313. Williams, J., de Geus, E., Blitz, L., 1994, ApJ, 428, 693
314. Williams, J., Blitz, L., Stark, A., 1995, ApJ, 451, 252
315. Williams, J., McKee, C., 1997, ApJ, 476, 166
316. Wilson, R., Jefferts, K., Penzias, A., 1970, ApJ, 161L, 43
317. Wolfire M.G., Hollenbach D., McKee C.F., 1995, ApJ 443, 152
318. Wolfire M.G., Hollenbach D., McKee C.F., 2003, ApJ 587, 278
319. Wolfire M.G., Hollenbach D., McKee C.F., 2010, ApJ 716, 1191
320. Wong, T., Hughes, A., Fukui, Y., et al. 2009, ApJ 696, 370
321. Zank, G., Matthaeus, W., 1990, PhRvL, 64, 1243